nuclear science and technology

Safety and Operational Monitoring of Nuclear Waste Repositories with Fibre-optic Sensing Systems (SOMOS)

Authors

P. Borgermans, S. Labat, B. Brichard, G. Volckaert – SCK•CEN (BE)
J. Vlekken, M. Voet – FOS&S, ID-FOS (BE)
J. Guttierrez, Pedro Corredera – CSIC (ES)

Final report

Contract No FIKW-CT2001-00190

Work performed as part of the European Atomic Energy Community's R&T specific programme Nuclear Energy 1998-2002 (Fifth Framework Programme), key action Nuclear Fission Safety Area: Safety of the fuel cycle

> Directorate-General for Research Euratom

Acknowledgements

The European Commission is acknowledged for having financed the SOMOS project as part of Euratom's Fifth Framework Programme (FP5).

The Instrumentation Group, Euridice and BR2 of SCK•CEN are acknowledged for their support in carrying out the irradiation experiments and in-situ installations in the underground laboratory HADES.

Executive summary

The objectives of the project consisted of a substantial contribution to the development of a long-term reliable fibre-optic monitoring system for nuclear waste repositories. The types of fibre-optic sensors were limited to three basic safety parameters to be measured: radiation level (integrated and distributed), temperature (distributed) and hydrogen sensing. The objectives were contained in the following work areas: specification of requirements and the development of a qualification methodology for long-term monitoring systems; development of suitable fibre-optic sensing systems for the three parameters, based on current technology and prototype systems; investigation of the potential for renewable sensor systems by placing the fibres for distributed dosimetry and temperature in small (stainless) tubes as an answer to long-term reliability and future improvements.

Based on preliminary studies on fibre-optic sensors for the measurement of radiation dose, temperature and hydrogen, fibre-optic monitoring systems were developed together with a qualification methodology fulfilling the requirements and operational constraints. The work was organised in several work packages consisting of theoretical and practical work structured around the qualification methodology and the three basic sensing systems. Important issues such as the operation in radiation fields for temperature sensing systems was addressed both in laboratory and in-situ work. Distributed or integrated dosimetry on the other hand was tested with respect to robustness for environmental parameters.

For the in-situ work, collaboration with existing underground laboratories and other EC projects was established for optimising the overall efficiency and relevance of the results. The performance was also compared to conventional systems, installed in parallel with the fibre-optic systems. The long-term aspects (which consist mainly of reliability and re-calibration issues) and the qualification was partly addressed by considering the potential for renewable sensor systems when optical fibres were placed in small tubes, which in turn were installed and buried in the vicinity of the actual (high-level) waste (in our project, this was simulated waste forms in the CORALUS experiment).

Temperature sensing

For temperature sensing, the focus was on the design and testing of carbon-reinforced Tower gratings, as in the first part of the project it could be concluded that the Tower gratings show the least sensitivity under radiation. The carbon coating results in a stiffer but mechanically more durable fibre, whereas classical fibre Bragg gratings are quite fragile. Furthermore, the interrogation system for a distributed temperature sensing network was developed, including dedicated data-acquisition software.

Hydrogen sensing

For hydrogen sensing, three prototypes have been designed, developed and tested in the presence of varying hydrogen concentrations. A first prototype was based on the change in reflection coefficient of a palladium-coated mirror. A second prototype employed fibre Bragg gratings where the swelling of a palladium coating due to hydrogen absorption causes

mechanical stresses which modify the characteristic wavelength of the Bragg grating. The third prototype employed the characteristic absorption peaks of hydrogen present in the fibre core. In the presence of hydrogen, a part of the hydrogen slowly diffuses into the fibre causing the absorption peak to increase in value. For all three prototypes of hydrogen sensors, adequate sensitivity and reversibility of the process were demonstrated.

Radiation sensing

Radiation sensing is performed through special doped fibres which show a first order (or even linear) increase of the radiation-induced optical attenuation around 1300 to 1500 nm when placed in a radiation field. The temperature dependence of the response is negligible in the envisaged operating range (20 to 90 °C), while the dose-rate dependence was demonstrated to be low in a region between 1 and 100 Gy/h.

In order to obtain distributed radiation sensing, the use of a high-resolution Optical Time Domain Reflectometer (OTDR) was attempted. Although the specifications, such as a high spatial resolution, high sensitivity and dynamic range seemed to be ideal for distributed measurements, results obtained were disappointing. Finally, distributed radiation sensing was abandoned for this project, mainly due to resource and time constraints at the end of the project.

In-situ integration

As part of the demonstration aspects of the SOMOS project, temperature and radiation sensing were planned using dedicated stainless steel tubes engineered and emplaced within the CORALUS tests in the HADES underground research laboratory in Belgium. Though the placement of optical fibres in capillary tubes is a mature technology in telecommunication systems, the particular set-up used is far more demanding. Mainly the fact that the capillary tubes were placed with several loops around the CORALUS test tubes imposed a lot more friction during emplacement. The (fragile) optical fibres used for radiation sensing proved to be impossible to inject fully given the local geometry of the CORALUS experiment. However, the carbon-reinforced Tower grating fibres for temperature sensing were successfully placed and benchmarked against the available classical temperature sensors.

Assessment of the applicability of the monitoring systems in nuclear waste repositories

Of the three sensing techniques investigated, the applicability of a distributed temperature monitoring system using fibre Bragg gratings is well demonstrated. The fact that these fibres can be installed and replaced at all times also guarantees the long-term usability, a property which differentiates this type of systems with classical sensors which can not be replaced after emplacement of waste forms (or it would be very costly to do so). The same advantage is in principle also valid for radiation sensing. Even though the demonstration failed in the in-situ integration tests, a careful design taking into account geometry constraints with placement of the capillary tubes should enable a successful deployment. For hydrogen sensing, where the qualification was valid in absence of radiation, the resulting monitoring system can at least be applied in areas of low radiation inside the repository. In any case, the results of this project should be considered in the overall design of possible monitoring systems for nuclear waste repositories.

Table of contents

| 1 | Intro | oduction | 1 |
|---|-------|---|------|
| | 1.1 | Background | 1 |
| | 1.2 | Objectives | 1 |
| | 1.3 | Methodology | 2 |
| 2 | Scie | ntific results | 3 |
| | 2.1 | Qualification of fibre-optic monitoring systems | |
| | 2.1. | Development of requirements for qualification of fibre-optic monitoring systems | 3 |
| | 2.1.2 | | |
| | 2.1.3 | 3 Operating principles for laboratory testing | 3 |
| | 2.1.4 | Installation and operation of a sensing network at selected sites | 9 |
| | 2.2 | Temperature sensing | |
| | 2.2. | 5 | |
| | 2.2.2 | r · · · · · · · · · · · · · · · · · · · | |
| | 2.2.3 | | |
| | 2.2.4 | | |
| | 2.3 | Hydrogen detection | |
| | 2.3. | r | |
| | 2.3.2 | 1 31 | |
| | 2.3.3 | | |
| | 2.3.4 | | |
| | 2.4 | Monitoring of radiation | |
| | 2.4. | - J | |
| | 2.4.2 | | |
| | 2.4.3 | | |
| | 2.4.4 | \mathcal{E} | |
| | 2.4.5 | 5 In-situ integration | . 52 |
| 3 | Asse | essment of results and conclusions | . 53 |
| 4 | Refe | erences | . 55 |
| 5 | Con | tacts | . 55 |
| A | PPEND | IX: Distributed fibre-optic sensing systems | 57 |
| | | uted temperature sensing using the Brillouin effect | |
| | | uted temperature sensing using the Raman effect. | |

1 Introduction

1.1 Background

Safe disposal of radioactive waste and spent nuclear fuel is considered to be a major challenge for the present generation independently of current and future scenarios of nuclear power use in different countries. Extensive research and project implementation efforts have been in place for several years in all leading industrial nations in order to enable a sustainable solution of this task. In Europe, repository experience for low and intermediate level waste exists in several countries. Further decisions regarding site selection, site confirmation and licensing as well as construction of geological repositories, especially for high-level waste and spent fuel, are still pending in many countries. According to the Joint Convention of 27 September 1997 on the Safety of Spent Fuel Management and on the Safety of Radioactive Waste Management, contracting parties committed themselves "to take the appropriate steps to aim to avoid imposing undue burdens on future generations". Due to the enormous complexity and to extremely long implementation periods of up to some decades of years, radioactive waste disposal projects require mature concepts developed well in advance and continuous effort in order to comply with the taken commitment.

Last, but not least, the availability of suitable monitoring systems has an essential social dimension in regard to public acceptance and confidence building providing a sufficient verification tool.

1.2 Objectives

According to IAEA-TECDOC-1208, monitoring of geological repositories for high-level nuclear waste is defined as

"continuous or periodic observations and measurements of engineering, environmental or radiological parameters, to help evaluate the behaviour of components of the repository system, or the impacts of the repository and its operation on the environment".

One of the issues to be solved is operational in-situ monitoring in geological repositories. Availability of appropriate monitoring tools is a major desire in order to ensure operational safety and in order to respond to manifold other safety-related demands. In-situ monitoring would provide the opportunity to increase confidence in the safety of the disposal system by verifying that the repository was evolving in the manner predicted. While such evaluation would cover a period of a few decades, at most, it would nevertheless be possible to verify within the near field of the repository, over this period, parameters such as temperature, geomechanical values etc. and compare them with earlier predictions. In this context, the availability of reliable monitoring systems and the remote control of the underground environment over several decades could be understood as a powerful quality-assurance tool in regard to repository planning. Such measurements will be unique in regard to verification of the behaviour of a specific site under the impact of the emplaced waste over relatively long time frames. Furthermore, in several countries retrievability options and/or additional performance assessment before repository closure are subject to national legislation or current planning scenarios or both. Thus, the request for in-situ monitoring is a logical consequence.

In addition, the objective of the proposed project responded directly to some lessons learned from tests in underground laboratories, in particular to the loss of a significant part of

measurement instrumentation in the case of sensor failure. Recognising that in principle all national strategies for geological disposal of high-level waste and spent nuclear fuel involve a sufficient phase of on-site conformation consisting of series of underground investigations and large-scale tests at the further disposal site, appropriate long-term reliable monitoring tools are a prerequisite for the successful completion of such efforts. They will support the improvement of the understanding, conceptualisation and modelling of the phenomena and processes expected to take place in the disposal system as a whole by gathering reliable data to be used in repository-performance assessments.

1.3 Methodology

The SOMOS project consists of four work packages which are summarised in the table below.

| WP | Title | Description | Partners |
|----|--|---|--------------------------|
| 1 | Qualification of fibre- optic monitoring systems | Determining the requirements for qualification of the sensors involved in the other work packages. Based on these requirements, a methodology for qualification will be developed for the handling of the individual sensors as well as the complete systems | SCK•CEN IDFOS CSIC |
| 2 | Temperature sensing | Monitoring the thermal evolution of an underground repository (including host rock and technical barriers) is crucial to evaluate the safety of the repository. The monitoring type envisaged is mainly multipoint along the fibre | IDFOS SCK•CEN |
| 3 | Hydrogen detection | Detecting gas concentration in an underground site is one major safety requirement. Multipoint/multivariable gas monitoring should be able to detect presence of H ₂ . Thus, in the framework of the recent work package, a multipoint monitoring system based on small microoptic cells and capable of resolving approximately 1 % of the lower explosive limit of several gases will be developed and tested | CSIC |
| 4 | Monitoring of radiation | During the operational and, if desired, the retrievable phase of a nuclear repository, it is crucial to monitor the performance of the chemical and physical barriers. This involves gamma radiation dosimetry in the close vicinity of the canisters. Thus, in this work package, special attention is put on the use of optical fibres as gamma dosimeters | SCK•CEN IDFOS |

The three detection areas are fairly independent in terms of R&D throughout the project. However, the integration of temperature and radiation sensing is one of the goals for the insitu testing.

2 Scientific results

2.1 Qualification of fibre-optic monitoring systems

2.1.1 Development of requirements for qualification of fibre-optic monitoring systems

The qualification of fibre-optic monitoring systems depends on the concept of storage facility, regulatory requirements for monitoring and site specific conditions. At present, no final concept or facility is operational; hence no firm requirements could be developed.

The possible requirements for monitoring were also the subject of an EC Thematic Network "On the role of monitoring in a phased approach to disposal". This exercise provides more information on requirements for monitoring in future systems. However, the most stringent requirements are to originate from a final concept and corresponding regulatory authorities.

The requirements for qualification in the SOMOS project are therefore based on previous research on potential concepts and the simulated HLW experiment of the CORALUS II project.

| | Unit | Value |
|-------------------------------|------|----------|
| Temperature range | °C | 30 to 90 |
| Length of sensing line | m | +/- 5,20 |
| Max. diameter of sensing line | mm | 2 |
| Number of curvatures | | 3 |
| Diameter of curvatures | mm | 300 |
| Dose rates | Gy/h | 0 to 150 |

2.1.2 Development of a methodology for qualification

The methodology for qualification is mainly based on operational constraints (emplacement, operation, verification and calibrations) as well as specific properties of operating environment (radiation levels and temperature) in the vicinity of high-level waste canisters.

This is addressed in the respective sections for the different sensors considered in this project.

2.1.3 Operating principles for laboratory testing

2.1.3.1 Temperature sensing

The temperature monitoring is performed using the Fibre Bragg Grating (FBG) sensors. Fibre Bragg Gratings are made by laterally exposing the core of a single-mode fibre to a periodic pattern of intense ultraviolet light. The exposure produces a permanent increase in the refractive index of the fibre's core, creating a fixed-index modulation according to the exposure pattern. This fixed index modulation is called a grating. At each periodic refraction change a small amount of light is reflected. All the reflected light signals combine coherently to one large reflection at a particular wavelength when the grating period is approximately half the input light's wavelength. This is referred to as the Bragg condition, and the wavelength at which this reflection occurs is called the Bragg wavelength. Light signals at wavelengths other than the Bragg wavelength, which are not phase matched, are essentially

transparent. This principle is shown in Figure 1. Therefore, light propagates through the grating with negligible attenuation or signal variation. Only those wavelengths that satisfy the Bragg condition are affected and strongly back-reflected. The ability to accurately preset and maintain the grating wavelength is a fundamental feature and advantage of fibre Bragg gratings. Gratings can also be designed to couple other phase-matched wavelengths out of the fibre core, into radiation and cladding modes for tailoring of the grating spectrum.

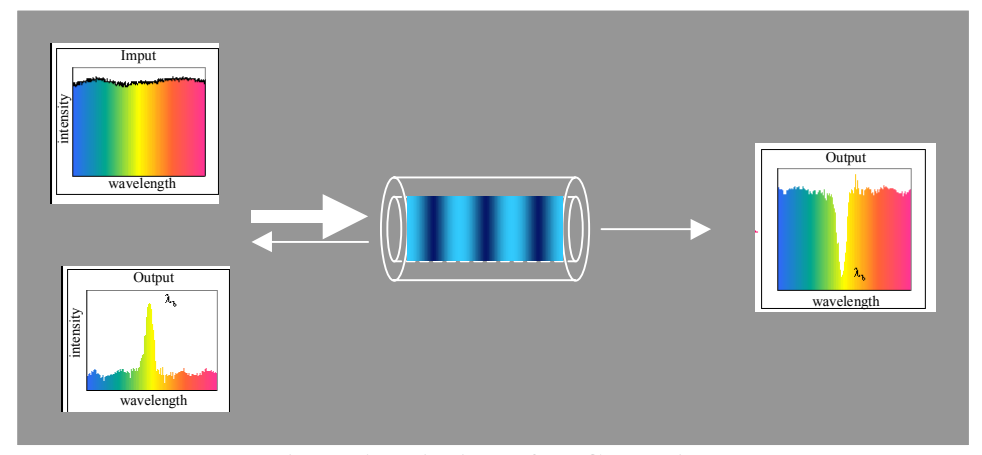


Figure 1: Principle of FBG working

The central wavelength of the reflected component satisfies the Bragg relation:

$$\lambda_b = 2 \cdot n_{eff} \cdot \Lambda$$
Equation 1

with n_{eff} the index of refraction and Λ the period of the index of refraction variation of the FBG. Due to the temperature and strain dependence of the parameters n and Λ , the wavelength of the reflected component will also change as function of temperature and/or strain.

From Equation 1 is clear that the Bragg wavelength depends on the effective index of refraction (n_{eff}) and on the pitch (Λ) of the grating. It is obvious that the grating pitch will be affected by changes in strain and temperature due to elongation or shortening of the optical fibre. But also the effective index of refraction is dependent both on temperature and strain due to internal stresses in the fibre core. Using Equation 1, the total shift in Bragg wavelength due to strain and temperature was derived by Butter and Hocker [Butter, CD; Hocker, GB (1978): Fibre-optics strain gauge. Applied Optics 17, nr. 18] and is given by:

$$\begin{split} \Delta \lambda_{_{B}} &= 2 \cdot (n_{_{eff}} \cdot \frac{\partial \Lambda}{\partial \epsilon} + \Lambda \cdot \frac{\partial n_{_{eff}}}{\partial \epsilon}) \cdot \Delta \epsilon + 2 \cdot (n_{_{eff}} \cdot \frac{\partial \Lambda}{\partial T} + \Lambda \cdot \frac{\partial n_{_{eff}}}{\partial T}) \cdot \Delta T \\ &\qquad \qquad \textbf{Equation 2} \end{split}$$

The first component of Equation 2 represents the effect of mechanical strain applied along the axis of an optical fibre with Bragg grating. It corresponds to a change in the grating spacing and a change in the refractive index; these terms can be written as follows. The first term of the strain component $2 \cdot n_{\text{eff}} \cdot \frac{\partial \Lambda}{\partial \epsilon}$ can be written as, using equation 1, $\frac{\lambda_B}{\Lambda} \cdot \frac{\partial \Lambda}{\partial \epsilon}$, in which

 $\frac{\partial \Lambda}{\Lambda} = \Delta \epsilon$. By introducing the following definition for the so-called **(effective) strain-optic constant** P:

$$P = -\frac{1}{n_{eff}} \cdot \frac{\partial n_{eff}}{\partial \epsilon}$$

Equation 3

This last term of the strain component finally becomes -P λ_B . Eventually, under the assumption of small strain variations (such that $\partial \varepsilon = \Delta \varepsilon$), the strain effect may be expressed as:

$$\Delta \lambda_{B} = \lambda_{B} \cdot (1 - P) \cdot \Delta \epsilon$$
Equation 4

where P can be calculated as:

$$P = \frac{n_{eff}^{2}}{2} \cdot [p_{12} - v \cdot (p_{11} + p_{12})]$$
Equation 5

in which p_{11} and p_{12} are components of the strain-optic tensor, and v is the Poisson's ratio of the optical fibre material. For a typical germano-silicate optical fibre $p_{11} = 0,113$, $p_{12} = 0,252$, v = 0,16, and $n_{eff} = 1,482$. Substitution of these parameters in Equation 5 and Equation 4 gives a value of the strain-optic coefficient P = 0,21. And the anticipated strain sensitivity at ~ 1300 nm is a 1,0 pm change as a result of applying $1\mu\epsilon$ (this is a strain of 10^{-6} mm/mm) to the Bragg grating. At ~ 1550 nm the Bragg wavelength λ_B will change 1,2 pm/ $\mu\epsilon$.

The second term in Equation 2 represents the effect of temperature on the Bragg wavelength. It corresponds to a thermal expansion of the Bragg grating and again a change in the refractive index. This fractional wavelength shift for a temperature change ΔT may be written as:

$$\Delta \lambda_{B} = \lambda_{B} \cdot (\alpha_{f} + \alpha_{n}) \cdot \Delta T$$

$$\Delta \lambda_{B} = \lambda_{B} \cdot \beta \cdot \Delta T$$
Equation 6

where $\alpha_f = \frac{1}{\Lambda} \cdot \frac{\partial \Lambda}{\partial T}$ is the thermal expansion coefficient of the optical fibre (approximately

0,55 x 10⁻⁶ 1/K for silica). The quantity $\alpha_n = \frac{1}{n_{eff}} \cdot \frac{\partial n_{eff}}{\partial T}$ represents the so-called **thermo-**

optic coefficient, which is approximately equal to 8,6 x 10^{-6} 1/K for the germania-doped, silica-core fibre. The coefficient α_f and α_n are combined in the **temperature coefficient** β . Clearly the index change is by far the dominant effect.

It now becomes apparent that any change in wavelength, associated with the action of an external perturbation to the grating, is the sum of strain and temperature terms. Therefore, in sensing applications where only one perturbation is of interest, the deconvolution of temperature and strain becomes necessary.

From Equation 4 it can be seen that the strain is directly encoded into a wavelength, which is an absolute parameter. Measurement interruption, by accident or intended, does not cause any problem, and does not ask for a new calibration, as is most often the case with classical strain gauges. It also appears that the result does not depend on the total light level; losses in the connecting fibres or optical couplers, or fluctuations in the power of the broadband light source have no influence. This is an important aspect when considering long-term field measurements. Furthermore, the wavelength-encoded nature of the output also facilitates wavelength division multiplexing. It allows the distribution of several gratings over a single optical fibre, by assigning each sensor to a different portion of the available spectrum of the light source.

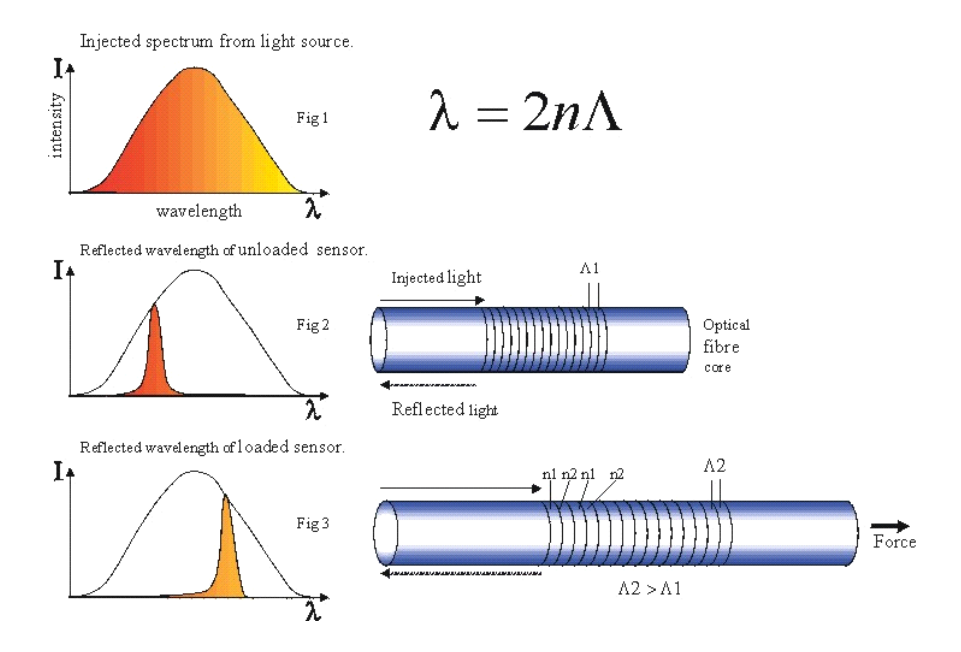


Figure 2: FBG response as function of strain

It finally needs to be mentioned that the FBG technology can also be used to measure other physical parameters than temperature and strain. Different sensors have already been developed at FOS&S and at other companies. The sensor can be seen as a transduction mechanism that strains a FBG in function of the monitored physical parameter. Examples of sensors are: hydrogen detection, water detection, displacement measurement, water pressure measurements, total pressure measurements, high-resolution strain measurement (0.1 microstrain).

For the application envisaged here, it is required that the FBGs also will be able to be insensitive to a certain degree for gamma radiation. In other words, the gamma radiation should not affect the temperature response of the FBGs too much. Therefore the FBG response to temperature will be verified as function of different parameters. The following parameters need to be taken into account:

- 1. Dose rate
- 2. Total dose
- 3. Temperature.

2.1.3.2 Hydrogen sensing

For hydrogen sensing, three different types of sensors are investigated.

A: The optical fibre as an intrinsic sensor element. The spectral absorption of an optical fibre exposed to gas mixtures with H2 concentrations of 2 and 4 % has been studied in the wavelength window from 1150 nm to 1700 nm. Several absorption peaks related to hydrogen are present. The main absorption peaks are located around 1245 nm and 1390 nm, but the latter is related to OH- ions and is not reversible. As the absorption peak at 1315 nm is not sensitive for low levels of H2 it is suitable to be used as reference to measure the relative changes in the peak at 1245 nm. The attenuation due to the uptake of H2 in the fibre is reversible.

<u>B: Pd semitransparent film sensors.</u> In this case an 18 nm Pd thickness film is deposited on a SiO₂ substrate. Either the transmittance or the reflectance can be used as a sensing mechanism. The sensibility of this sensor is independent of the wavelength in a wide range of wavelengths (1200 to 1600 nm).

<u>C: Pd-coated fibre Bragg gratings (FBG)</u>. A Pd layer deposited over a fibre Bragg grating is the essential part of the design. When a Pd film absorbs hydrogen it expands because Pd converts to PdH_X which has a larger volume. When FBG Pd coated absorbs H_2 , the mechanical expansion stretches the fibre which causes a change in the characteristic reflected wavelength of the FBG due to the induced (extra) strain in the fibre. In order to enhance the strain produced by the H_2 absorption, a small diameter FBG must be used (20-30 μ m).

2.1.3.3 Radiation sensing

The main sensing principle for radiation with optical fibres is the radiation induced optical attenuation (RIA).

Radiation induced attenuation in optical fibres has been extensively studied during the past decades as they offer distinct advantages for telecommunication applications and as sensors for a wide range of measurands. Most of the efforts were devoted to radiation hardness in nuclear or space applications, but their potential for dosimetry has been investigated too. In this respect, the optical fibre acts as sensing medium for radiation through induced changes of the optical absorption in the fibre waveguide. For most of these experiments, silica based fibres are used with a variety of dopants for the core and cladding, as opposed to scintillating fibres, which are mainly based on plastics or organic materials for use in high energy physics experiments.

The dynamic response for a given interrogating wavelength is the sum of different contributions from the underlying absorption bands kinetics. A number of papers treated the modelling of the combined ("envelope") kinetic behaviour of the RIA at one or a few wavelengths during irradiation and the recovery after irradiation. Obviously, a simple model for this is of interest for dosimetry applications where the dose is measured on-line during irradiation. The recovery or "fading" dynamics are important for off-line dosimetry or varying dose-rate regimes.

The basic equation for measuring the radiation induced attenuation is:

$$A(\lambda,t) = -\frac{10}{L} \left[Log \left(\frac{P_T(\lambda,t)}{P_T^{O}(\lambda)} \right) - Log \left(\frac{P_R(\lambda,t)}{P_R^{O}(\lambda)} \right) \right] \quad [dB/m]$$

Subscript R and T stand for the reference (unirradiated) and test (irradiated) fibres respectively whereas the superscript o refers to the average value before irradiation. L is the total irradiated length of the fibre. $P_{T}(\lambda,t)$ and $P_{R}(\lambda,t)$ are the optical output powers during the irradiation in the test and the reference fibres respectively, at time t and wavelength λ . A schematic overview for measuring the optical attenuation is given in the figure below:

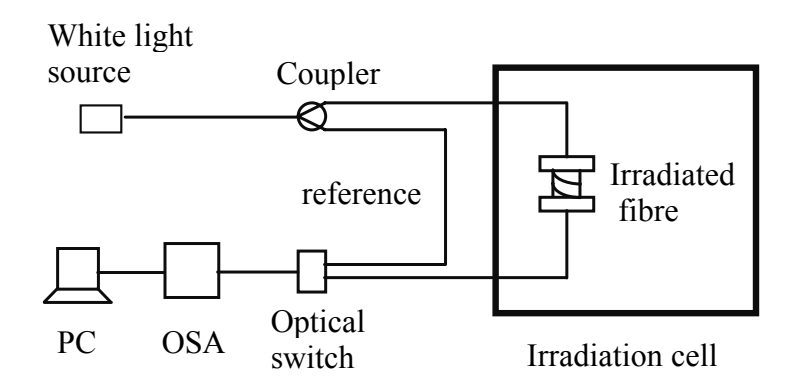


Figure 3: Principle for measuring the radiation-induced attenuation

In terms of material parameters, the radiation induced absorption can be formally represented by the simplified expression

$$A(E,t) = \sum_{i} k_{i}(t) \Psi_{i}(E) \quad [dB/m]$$

In this expression the wavelength is replaced by the corresponding photon energy E, which is a fundamental (material) parameter for the absorption band position $\Psi_i(E)$ and shape. E is calculated as $E[eV] = 1024 / \lambda [nm]$.

The absorption bands are further supposed to be time-invariant with respect to their shape and position, and the corresponding amplitudes $k_i(t)$ to contain all time related dependencies. The factors $k_i(t)$ therefore incorporate all the effects of temperature, photo bleaching, dose rate, dose and annealing – in general the irradiation and environmental history. The position, width and shape of these radiation induced absorption bands are characteristic for the fibre composition, fabrication method and radiation type.

In order to perform radiation sensing (dose reconstruction) from the induced attenuation, alternative estimators for the dose are pursued by considering the signals at different wavelengths. Generally, the equation for A(E,t) then becomes a set of equations where elimination of the unwanted parameters and annealing (fading) may be possible. For this idea to effectively work, the underlying absorption band characteristics need to contain sufficient mutual independence with respect to the unwanted, annealing related parameters.

2.1.4 Installation and operation of a sensing network at selected sites

The installation target was the CORALUS II experiment, which is considered to be the most representative with respect to final disposal and monitoring for this project. Only temperature and radiation monitoring was foreseen for the SOMOS project as hydrogen sensing would have required more resources and time due to regulations of safety.

Results for the in-situ work is presented in 2.2.4 In-situ installation and operation of a sensing network and 2.4.5 In-situ integration.

2.2 Temperature sensing

2.2.1 Evaluation of existing fibre-optic systems for thermal monitoring

2.2.1.1 Evaluation and performance check of existing systems operation and investigation of an in-situ pilot scale network

Some other fibre-optical sensing technologies that might be considered as competitive with sensing based on Fibre Bragg Gratings have been investigated.

2.2.1.1.1 Distributed temperature sensing using Raman effect

The Fibre-optic Distributed Temperature Sensing (DTS) method using the Raman effect was developed at the beginning of the nineteen eighties at Southampton University in England, UK. The DTS method is based on optical time-domain reflectometry (OTDR) and uses a technique derived from telecommunication cable testing.

In the DTS technique, a pulsed laser is coupled to an optical fibre through a directional coupler. Due to the interaction between this laser pulse and the fibre, different light components will be backscattered. One of these components is the Raman component which can be used for temperature measurements. The signals are recorded with a time resolving power what allows to resolve the temperature and distance simultaneously.

2.2.1.1.2 Distributed temperature monitoring using distributed Brillouin scattering

This technology makes use of a similar set-up as the DTS measurements but in this case the Brillouin scattered light is analysed. Brillouin scattering occurs by an interaction between a high-coherence incident light and an acoustic wave generated by the incident light in an optical fibre. The Brillouin scattered light frequency is shifted from incident light frequency by an amount determined by the material. This frequency is called Brillouin frequency shift and it is determined by the refractive index, the acoustic wave velocity and the wavelength of incident light. The Brillouin frequency shift is in proportion to the change of strain/temperature.

2.2.1.1.3 Comparison with fibre Bragg grating sensing

In Appendix A, a comparison has been made between Raman, Brillouin and FBG temperature sensing.

2.2.1.2 Specification of system upgrades

Within the SOMOS project, it has been chosen to use the FBG technology for the temperature measurements. Main reason for this is the high spatial resolution (< 0,1 m) that is required for the application. This spatial resolution can only be achieved using the FBG technology.

In general, FBGs are manufactured using a standard procedure described in Annex B-I. As can be observed, this procedure requires a step where the outer coating of the fibre needs to be stripped. This lowers the strength of the FBG. Typically, a standard FBG can sustain tension forces up to 1 kg. This corresponds to a strain of more or less 1 %. As a consequence, the fibre is very damage sensitive for axial loads. Especially on the long term, this can cause problems. It is therefore aimed to increase this strength.

In order to accomplish this, special FBGs will be used which are manufactured using a procedure that does not require the stripping process. Two possible methods can be considered:

- a) UV-transparent coated fibre gratings
- b) Tower gratings.

Both methods are explained in Annex B-II and B-III respectively. It needs to be emphasised that the UV-transparent coated fibre grating technology is today in a very preliminary phase and are therefore not considered. Only the tower FBGs have been considered. These FBGs have the following important advantages:

- 1) High strength (up to 5 % peak strain what corresponds to 5 kg axial peak load)
- 2) FBGs can be put in series without the use of splices.

Disadvantage is however that the reflectivity of this type of FBGs is rather low (5-10 %) what requires the development of an interrogation system with a high dynamic range in order to be able to interrogate the different FBGs with a good signal noise ratio.

It also needs to be emphasized that the cross sensitivity between strain and temperature of the FBGs also requires some special attention. In order to assure good temperature accuracy, the fibre should all the time be positioned into a strain free state. It's however very difficult to insert the fibre inside the stainless steel capillary without leaving the fibre in an unstrained position. Especially due to the curvature problems can be expected. The curvatures can form an obstacle and cause some friction between the fibre and tube. Furthermore, thermal expansion of these capillaries might induce strain effects on the fibre what might result into breakage or measurement errors due to the cross sensitivities between strain and temperature.

It is therefore envisaged to increase the stiffness of the fibre/cable such that the temperature measurements are much less sensitive to these effects.

Finally, the FBGs also need to be resistant against gamma radiation to a certain degree. The radiation sensitivity of FBGs strongly depends on the chemical composition of the fibre and the photo-sensitation technique used for writing the FBGs. According to A. Gusarov et al. [A. Gusarov, D. Starodubov, A. Fernandez Fernandez, F. Berghmans, O. Deparis, Y. Defosse, M. Décreton, P. Mégret and M. Blondel: "Design of a radiation hard optical fibre Bragg grating

temperature sensor" in SPIE Conf. on Photonics for Space and Enhanced Radiation Environments, Vol. 3852, pp. 43-50, 1999], the sensitivity to gamma radiation of FBGs written in hydrogen-loaded telecom fibres was founded to be higher. The lowest radiation sensitivity is achieved with standard highly Ge-doped photosensitive fibre, without any pre-or post-fabrication treatment.

2.2.2 Specification for in-situ installation and operation

2.2.2.1 Specification of the individual sensors

Two different types of FBG sensors have been considered:

- 1) Tower gratings
- 2) Carbon-reinforced Tower gratings.

The specifications of the tower FBGs are shown in Table 1.

| | Unit | Value |
|-------------------------|-------|---------------|
| FBG type | - | TYPE I |
| Temperature range | °C | - 20 to 300 |
| Temperature sensitivity | pm/°C | 9.8 |
| Strain sensitivity | pm/μ□ | 1,2 |
| Bandwidth | pm | 200-300 |
| Length of FBG | mm | +/- 10 |
| Reflectivity | % | < 10 |
| Side lob suppression | dB | > 20 |
| Maximum peak load | kg | 5 |
| Photosensitivity | - | High Ge-doped |
| | | 15 mol% |

Table 1: Specification of Tower FBGs

Besides the tower grating, a new sensor has been developed: carbon reinforced tower grating. The design of the carbon-reinforced tower grating is shown is Figure 4. It consists of a tower grating surrounded with different carbon fibres. This all is kept together using a special epoxy resin that can sustain temperatures up to 150 °C.

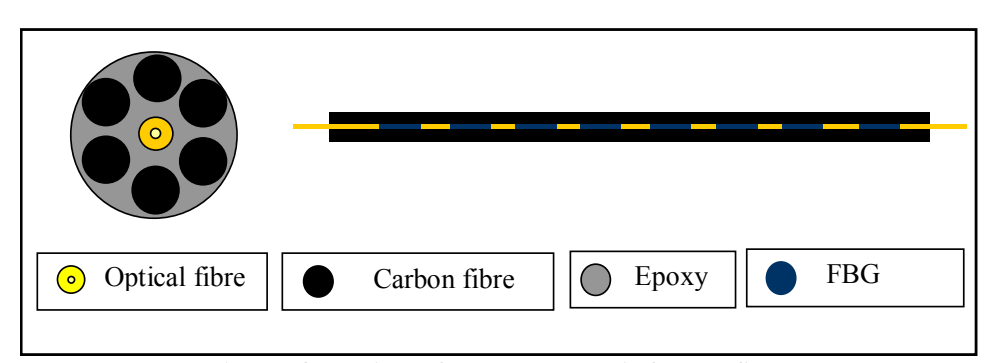


Figure 4: Design of the carbon-reinforced fibre

The advantages of the reinforcement are:

o It protects the fibre from breakage and sharp particles onto for example the capillary edges.

- Due to the cross sensitivity between strain and temperature influence on the FBG response, the reinforcement should also eliminate the possible strain influences on the FBG.
- It provides stiffness to the fibre such that the fibre can precisely be inserted into the capillary by pushing from one side. This will allow positioning the FBG exactly on the required position.

2.2.2.2 Specification of sensing networks

As indicated above, it has been decided to use the tower gratings for the temperature sensing system. These gratings are written during the drawing of the fibre itself into high Ge-doped single mode fibre. The writing process only takes one laser shot, resulting into a low reflectivity grating (< 10 %). Because of the low reflectivity, the interrogation cannot be performed using a low cost standard interrogation instruments. Therefore it has been decided to build a unit ourselves. A modification in the work contents of WP2 has therefore been asked – see letter from 16 March 2004. The unit will have the following characteristics:

- a) High dynamic range of 20 dB in order to make interrogation of tower gratings possible.
- b) Allow periodically spectrum measurements to perform peak shape control of the FBGs and signal noise calculations.
- c) Have a high stability and show no signal drift in time. This can be achieved by the possible use of special calibrations cells.
- d) Multiplexing of sensors in series and in parallel configuration must be possible.
- e) Have a temperature operating range between 10 and 40 °C.
- f) Measure up to 20 FBGs/optical line
- g) Have a wavelength read-out resolution of 1pm. This corresponds to a temperature resolution of 0,1 °C.
- h) Have an absolute wavelength accuracy of +/- 20 pm
- i) Allow autonomous data logging and visualise results in graph mode.

2.2.2.3 Definition of design rules

The complete system should be designed such that a reliable working of the sensor and interrogator can be expected. With respect to the interrogation system, the components that will be used should be qualified according to general accepted industrial norms. For the sensors it is required that the production can be performed using a fully automatic controlled process such that the repeatability of different production lots can be assured.

2.2.3 Development of system prototypes

2.2.3.1 Design of sensors and sensing networks based on the design rules

The design principle of the sensing network is shown in Figure 5. The interrogation system exists of a broadband light source that couples the light through a 2-by-2 coupler into the fibre where the FBGs (temperature sensors) will reflect different components. This same coupler guides the reflected light, coming from the different FBGs, into an Optical Spectrum Analyser (OSA) module where the spectrum is recorded and the different peak wavelengths are calculated. In order to allow multiplexing in parallel, an optical switch needs to be integrated

such that 8 different sensing fibres can be interrogated sequentially. The control of the measurement system as well as the wavelength to temperature conversion is established using a graphical user interface that can be controlled using a laptop or desktop PC.

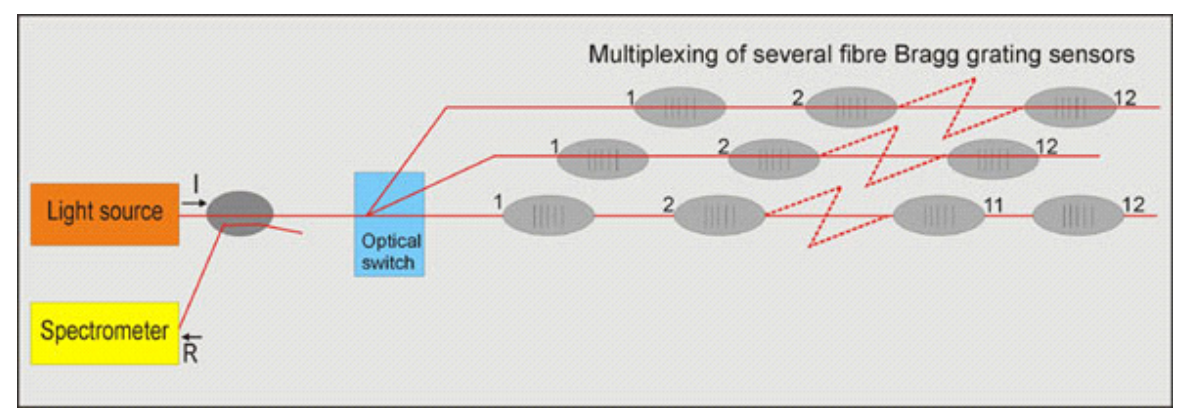


Figure 5: Working principle of the fibre-optic measurement system

2.2.3.2 Fabrication of the sensor prototype

The carbon-reinforced tower grating has been produced using a standard Pultrusion process. Figure 6 shows a schematic diagram of the process. Different carbon fibres and the Tower grating fibre with a diameter of 266 μ m are pulled through a epoxy impregnation bath (epoxy resin). The glass fibre is positioned at the centre. Subsequently, the fibres go through a shaping die with a diameter between 1,4 and 2 mm and are subsequently cured to harden out the epoxy resin. The resulting part is a carbon reinforced sensing fibre with a diameter ranging from 1,4 to 2 mm.

Figure 7 shows the used production set-up for the sensor prototype. The used set-up is a fully automated process and allows the fabrication of very long lengths, up to several km if required. The system is computer controlled assuring stable production parameters and a good repeatability between different production lots.

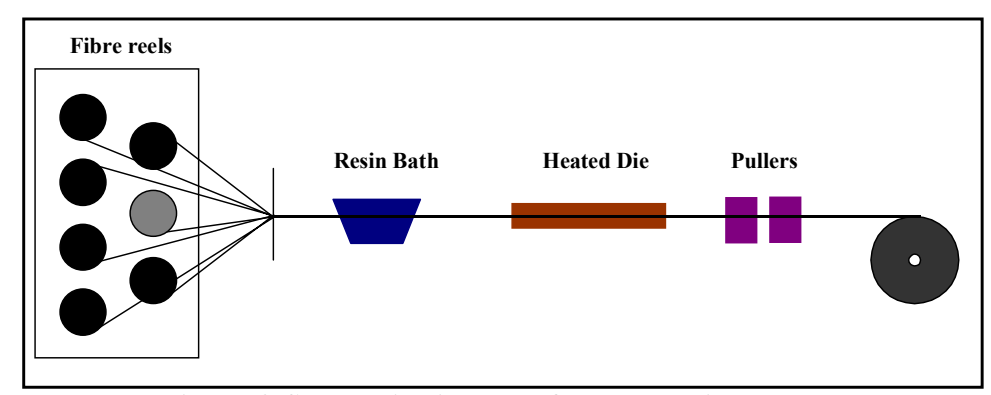


Figure 6: Schematic diagram of the Pultrusion process

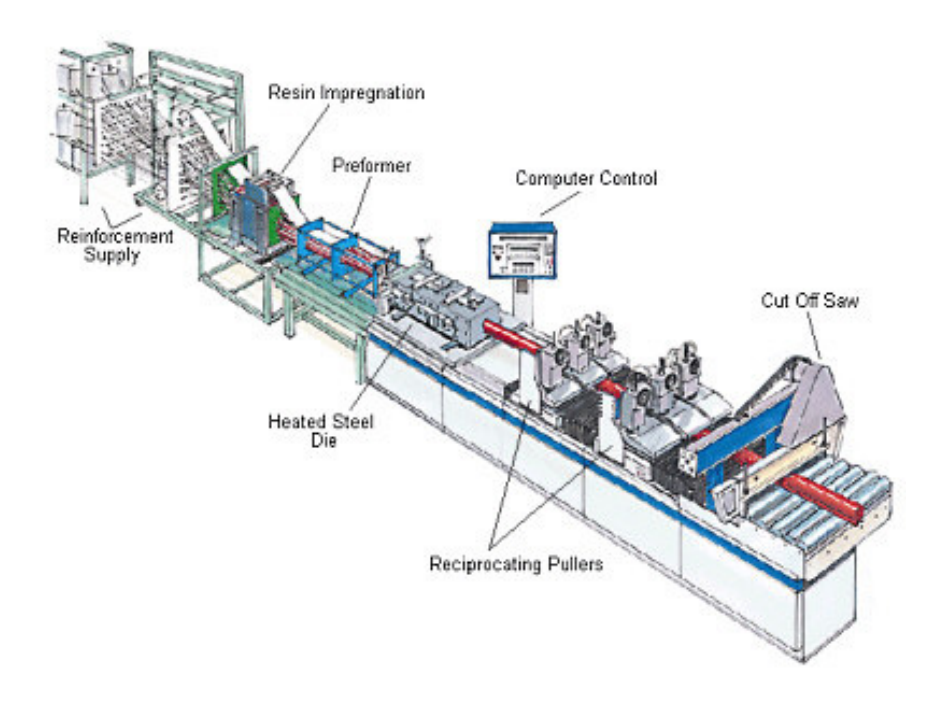


Figure 7: Production set-up of the Pultrusion process

In total three different types of carbon cables have been produced. These differ due to the used carbon fibre, optical fibre or epoxy, resulting in different specifications. Table 2 shows the characteristics of the carbon cable type 1. This type of carbon cable is also further considered for the CORALUS experiment. For the reinforcement of carbon cable 1, HS-carbon fibres have been used in combination with epoxy resin.

| Type carbon fibre | HS-carbon | | |
|--|------------------------------|--|--|
| Fibre type | Tower fibre grating | | |
| Diameter | 1,5 mm | | |
| Tension strength of the carbon fibre | 600-3300 MPa | | |
| Elasticity modulus of the carbon fibre | 125 GPa | | |
| Maximum elongation | 2 % | | |
| Density | 1,51,6 g/cm ³ | | |
| Thermal expansion | < 0,5 x 10 ⁻⁶ /°C | | |
| Resin type | Epoxy resin | | |

Table 2: Specifications of the carbon cable type 1

2.2.3.3 Fabrication of the interrogator prototype

A prototype has been fabricated according to the design shown in Figure 5. The interrogator prototype will have the name 'FBG-Scan 408'. The optical block diagram of the prototype interrogator is shown in Figure 8.

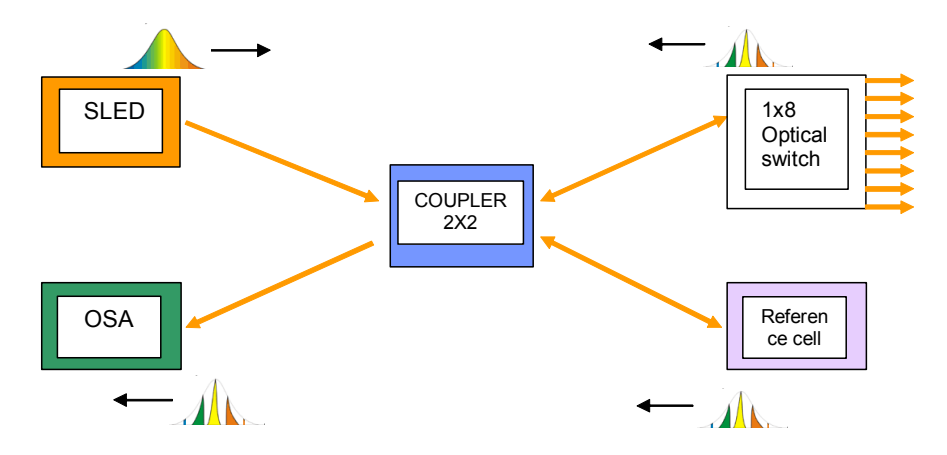


Figure 8: Block diagram of the interrogator prototype

The system consists of the following components:

1. Super Luminescent Emitting Diode (SLED). This is a high power broadband light source that illuminates the optical inputs of the optical switch and a reference cell after passing a 2 by 2 coupler. The output power of the SLED is 1 mW and the spectrum has a bandwidth of 40 nm, centred at 1550 nm. The spectrum modulation is below 0,2 dB. Figure 9 shows a typical spectrum of the used SLED.

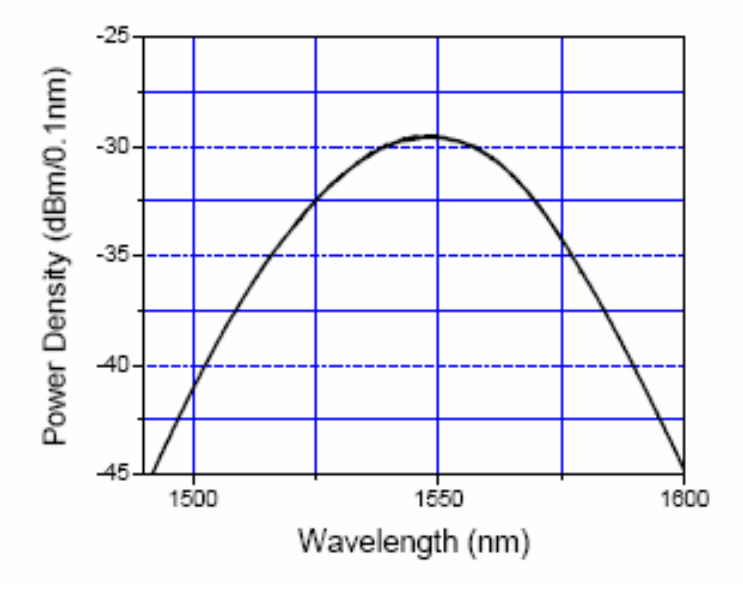


Figure 9: Power density spectrum of SLED

2. Optical switch that allows the multiplexing of 8 fibres in parallel. The optical switch is a bi-directional switch. The optical characteristics are shown in Table 3.

| Insertion loss | < 1 dB |
|-----------------------------------|--------------|
| Repeatability | +/- 0.02 dB |
| Polarization Dependent Loss (PDL) | < 0.1 dB |
| Crosstalk | < – 50 dB |
| Return loss | < – 50 dB |
| Wavelength range | 1520-1625 nm |
| Input Optical Power | < 20 dBm |

Table 3: Optical characteristics optical switch

- 3. The reference cell used to calibrate the miniaturised spectrum analyser. The reference cell consists of a double Fibre Bragg Grating. The first FBG at the beginning of the spectrum (reference grating 1 around 1529 nm) and the second FBG at the end of the spectrum (reference grating 2 around 1571 nm). Both gratings are housed in an athermal package in order to keep the reflected wavelengths stable over the complete operating temperature range of the interrogator. The athermal packaging assures that the intrinsic temperature response of the FBG is compensated by applying a negative strain to the FBG with increasing temperature. The wavelength stability of the reference grating is better than 15 pm over the operating temperature range of the interrogator (between 10 and 40 °C).
- 4. Miniaturised optical spectrum analyser (OSA) which analyses the reflected signals coming from the sensing fibres and the reference cell. The miniaturised spectrum analyser makes use of a MEMS tuneable filter with a very narrow line width of 1,8 to 3,5 GHz and a Finesse of 3000 to 5000. Figure 10 shows a typical transmission spectrum of the tuneable filter. The specifications of the miniaturised spectrum analyser are shown in Table 4.

5.

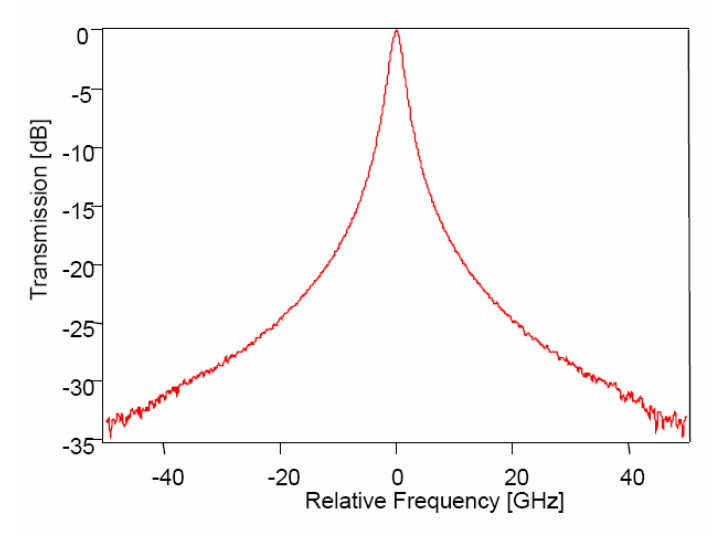


Figure 10: Transmission spectrum of tunable filter

| | Unit | Value |
|------------------------------|------|-----------|
| Operating temperature | °C | - 5 to 70 |
| Wavelength range | nm | 1530-1570 |
| Relative wavelength accuracy | pm | 80 |
| Wavelength resolution | Pm | 1 |
| Filter line width | GHz | 1,8-3,5 |
| Finesse | - | 3000-5000 |
| Absolute power accuracy | dB | 0,5 |
| Relative power accuracy | dB | 0,25 |
| Power range | dBm | - 50-0 |

Table 4: Specifications miniaturised optical spectrum analyser (OSA)

As can be observed, the miniaturised spectrum analyser covers a wavelength range between 1530 and 1570 nm. This broad range makes multiplexing of the sensors in a series configuration possible. Furthermore, the miniaturised spectrum analyser has a relative wavelength accuracy of 80 pm. In order to reduce this value, a special calibration procedure is used using the 2 reference signals. A correction can be applied using these reference gratings according to the following formula:

$$\lambda_{\text{cal}} = \lambda_1^{\text{a}} + \frac{\lambda - \lambda_1^{\text{m}}}{\lambda_2^{\text{m}} - \lambda_1^{\text{m}}}.(\lambda_2^{\text{a}} - \lambda_1^{\text{a}})$$

with:

- λ_{cal} the calibrated wavelength
- λ_1^a the absolute wavelength of reference grating 1 (at the beginning of the spectrum)
- λ_2^a the absolute wavelength of reference grating 2 (at the end of the spectrum)
- \bullet λ_1^m the measured wavelength of reference grating 1 according to the OM1 unit
- λ_2^m the measured wavelength of reference grating 2 according to the OM1 unit
- lacktriangledown λ the measured wavelength according to the OM1 unit of the to determining calibrated wavelength

Using this correction procedure, the absolute wavelength accuracy is expected to be lower than 35 pm. The relative wavelength accuracy is expected to be better than 20 pm.

Figure 11 shows the interior of the interrogation system. On the right side, the 1 x 8 optical switch is located. It is driven using a PCMCIA DIO24 digital input/output card in a laptop. At the left side we have the miniaturised spectrum analyser on the bottom with on top the electronic board for control and power supply of the SLED and the spectrum analyser. The board is described in more detail in Annex C. The control of the miniaturised spectrum analyser happens via an RS232 connector on the electronic board, also visible in the picture. It has to be connected further to a laptop. The complete system requires a 12 VDC input.

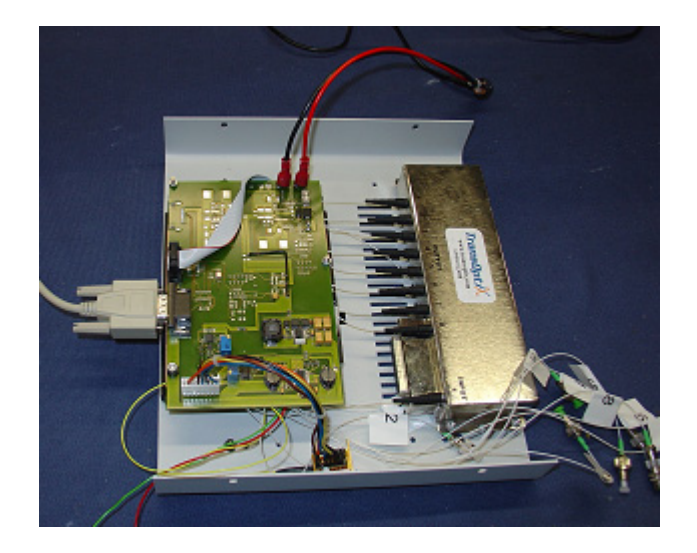


Figure 11: Photo of interior of the interrogator prototype

Figure 12 shows a photo of the front panel of the interrogator prototype. The front panel contains the following components:

- 1. LED for power indication
- 2. 8 optical inputs for FC/APC connectors.



Figure 12: Photo of the front panel of the interrogator prototype

The rear panel is shown in Figure 13. The rear panel contains the following components:

- 1. RS232 Connector to control the spectrum analyser (Baud rate is 115200 bits/second)
- 2. DC-in low voltage input connector for transformer
- 3. Digital input connector to control the optical switch inside the unit.
- 4. On/off switch to turn the device on and off.



Figure 13: Photo of the rear panel of the interrogator prototype

In order to control the system, a software programme written in Labview 6.1 has been developed. The interface consists of three tab pages: 'Wavelengths', 'Spectrum' and Temperature. The wavelengths tab is used when wavelengths need to be recorded as function of time. The spectrum tab is used to view the complete spectrum of the reflected wavelengths. The temperature tab allows converting the wavelength measurements to temperature values. All tab functions are explained below.

Figure 14 shows the interface of the 'Wavelength' tab. The 'Wavelength' tab contains the following elements:

- Chart display: Displays measured wavelengths [nm] as function of time. The wavelengths are expressed in nanometers.
- Display channel: defines which channel will be visualized on the chart display.
- Graph palette: can be used for changing scaling and formatting of the graph. It is also possible to adjust the axis scale manually by clicking on a value and fill in the desired value.
- Channel: indicates the current position of the optical switch.
- Optical switch settings: The operator can choose between manual and automatic switching by toggling the "auto" or "manual" button. When "manual" switching is chosen, the operator can switch between the different channels simply by using the "channel" control. If "automatic" switching is chosen, the operator can select two channels between which the optical switch will cycle continuously.
- Cycle time: The cycle time defines the pause in seconds between two complete cycles when auto switching has been selected. This control can be used when for instance only 1 measurement cycle/hour needs to be performed. If manual switching is selected, "cycle time" is not functional.
- Table: Displays the real-time wavelengths and corresponding power levels for each wavelength peak of the current channel.
- File name to save: Enter the directory and name of the data file. Click the file icon to browse. If the filename does not exist then a new file will be created. If the filename does exist then data is appended to the end of the existing file. Each measured channel will be saved under the defined file name extended with the channel number (e.g. wavelengths-1.txt).
- Save: Allows saving data to a txt file defined by the 'file name to save' control. If save function is activated, the 'Save' button will be red indicated and display 'saving'. Each time a measurement has been performed, the data is saved into a txt file.
- Stop button: Allows stopping the software programme.

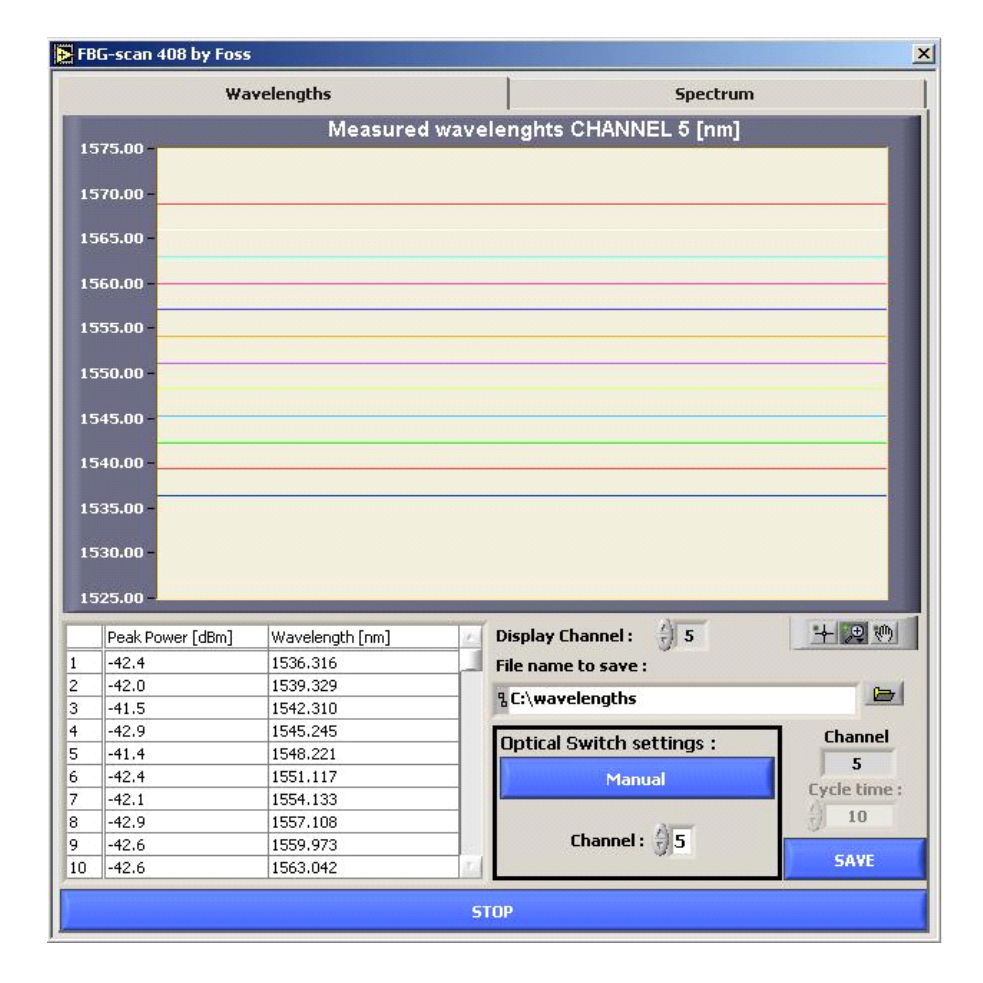


Figure 14: Software interface – Tab 1 'Wavelengths'

The 'Spectrum' tab is shown in Figure 15. This tab is created for diagnostics and will therefore only support manual switching. It contains the following elements:

- Chart Display: Displays the power spectrum of the reflected signal as function of the wavelength. The wavelengths are expressed in nanometers and the power in dBm.
- Graph Palette: Can be used for changing scaling and formatting of the graph. It is also possible to adjust the axis scale manually by clicking on a value and fill in the desired value.
- Channel: The operator can in this tab not choose between manual and automatic switching. Switching can only be performed in the manual mode. The operator can switch between the different channels simply by using the "channel" control.
- File name to save spectrum: Enter the directory and name of data file. Click the file icon to browse. If the filename does not exist then a new file will be created. If the filename does exist the software asks if the existing file may be overwritten. Note that the software automatically will add an extension after the saved file name in order to indicate the channel that has been measured.
- Snapshot: Allows saving one spectrum to the txt file indicated in 'File name to save spectrum' control. Note that this save function only records one scan.
- Decimation factor: This parameter determines the wavelength resolution with which the spectrum is shown. The higher this parameter, the lower the resolution. Note that low decimation factors result in slow measurement updates.
- Stop button: Allows stopping the software programme.

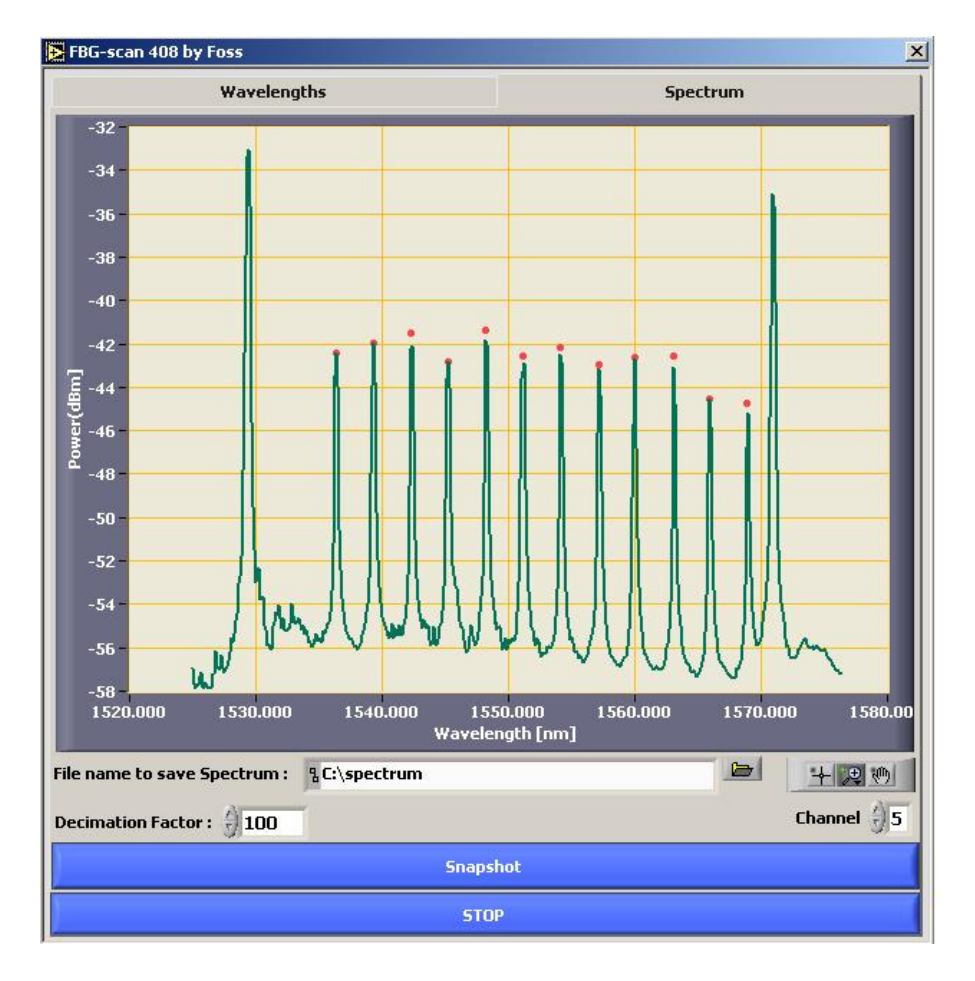


Figure 15: Software interface – Tab 2 'Spectrum'

The 'Temperature' tab is shown in Figure 16. This tab is created for converting the wavelength data to temperature data. It contains the following elements:

- Chart display: Displays temperatures [°C or °F] as a function of time. The wavelengths are expressed °Celsius or °Fahrenheit as selected with the Celsius and Fahrenheit control button. The displayed value will be updated every second (1 Hz scan rate).
- Table: Displays the real-time wavelengths and corresponding power levels for each wavelength peak. The temperature will be calculated from the nominal wavelength parameter and the sensitivity parameter (Both values need to be defined to calculate the temperature). The distance is an informative number (does not need to be defined).
- Adjust settings: To insert the parameters for the nominal wavelength and the sensitivity, the measurements need to be stopped to edit the table. This can be done by pushing the 'Adjust settings' button. The button name changes to 'Edit settings' and all other functions will be disabled. When finished with editing, push on the 'Edit settings' button and the measurements will resume with the new parameters.
- Load settings: Allows loading a file containing the set-up configuration for the temperature measurement.
- Save settings: Allows saving a file with the parameters for the temperature conversion.
- Celsius [°C]/Fahrenheit [°F]: Allows switching the units of the temperature readings from Celsius [°C] to Fahrenheit [°F] and visa versa.
- Save: Allows saving data to txt file indicated in the 'file name to save' control. If save function is activated, the 'Saving' button will be red indicated. It needs to be

- mentioned that when the user toggles between the different tab functions when saving is active, this will stop saving.
- Save temperature: Enter the directory and name of the data file wherein the temperatures will be saved. Click the file icon to browse. If the filename does not exist then a new file will be created. If the filename does exist then data is appended to the end of the existing file.
- Stop button: Allows stopping the software programme.
- Command bar: Indicates which operation is being performed on the FBG-scan 408. Error messages will be displayed if errors occur.

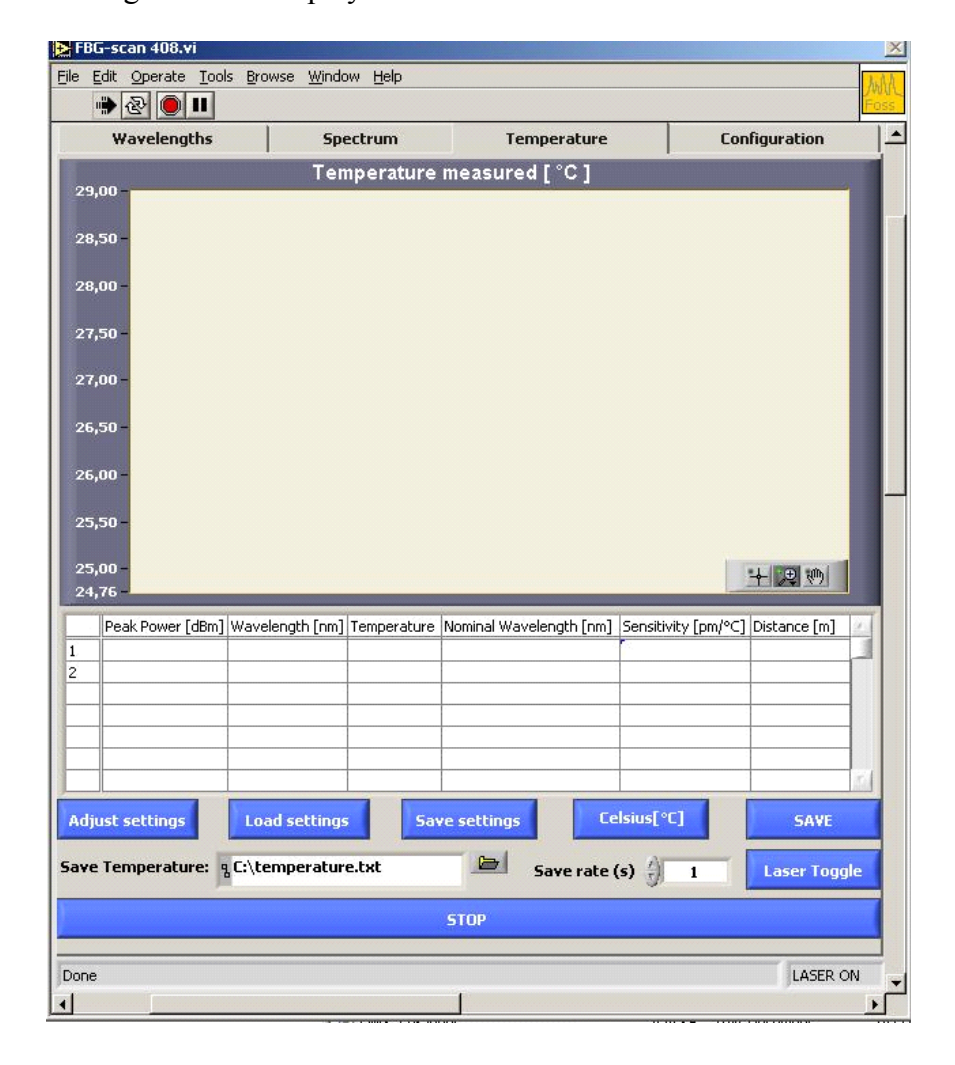


Figure 16: Software interface – Tab 3 'Temperature'

2.2.3.4 Evaluation sensor prototypes

Two different experiments have been performed in order to demonstrate the suitability of the carbon reinforced tower grating as temperature cable. In a first experiment, a temperature calibration has been performed. The temperature is changed from 10 °C up to 80 °C in steps of 10 °C. Each time thermal equilibrium has been reached, the wavelength has been recorded. The result of this experiment is shown in Figure 17. As can be seen, a good linear relation is obtained for all three FBGs. Even more, the different response curves are almost identical indicating that the process is well controlled. As can be observed, the temperature sensitivity for all three FBG is around 9,7-9,8 pm/°C. This is almost exactly the same as the temperature

sensitivity of the naked FBG which has been measured to be equal to 9.8 pm/°C. Hence, it can be concluded that the thermal expansion of the carbon reinforcement almost induce no strain to the tower grating, what was also expected due to the low thermal expansion coefficient as indicated in Table 2.

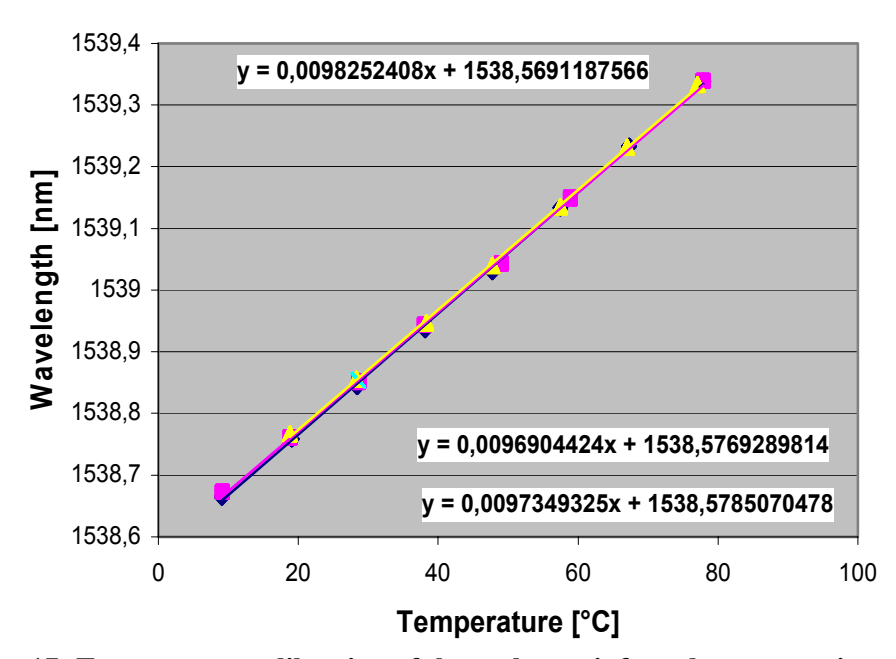


Figure 17: Temperature calibration of the carbon reinforced tower grating type 1

In a second experiment, a strain calibration has been performed. The carbon cable type 1 has been put under different load levels, ranging from 0 up to 10 kg. The result is shown in Figure 18. As can be observed, a good linear behaviour between wavelength and load can be observed with a sensitivity of 52 pm/kg. Since the sensitivity of the naked FBG is much higher, around 12 nm/kg, it can be concluded that the strain isolation is working very well. Furthermore, taking into account the strain sensitivity of the naked FBG of 1,2 pm/µstrain it can be calculated that the experimental elasticity modulus of the carbon reinforced tower grating is equal to 130 GPa. This is in good correspondence with the specified value of 125 GPa (Table 2).

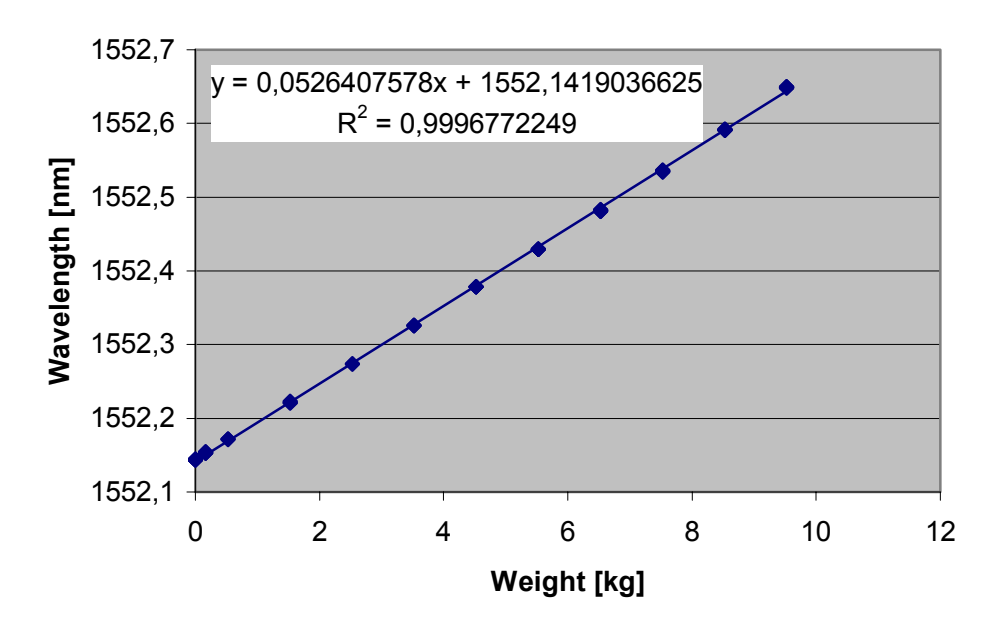


Figure 18: Load calibration of the carbon reinforced tower grating type 1

More tests have been performed with other types of carbon fibre and resin material, but not included here. It could be observed that temperature sensitivity can slightly be tuned by choosing the proper carbon or resin materials.

Furthermore, the influence of gamma radiation on the stability of the sensors has been tested. These experiments have been performed using the RITA installation at SCK. Figure 19 shows the measurement set-up. The system consists of a vertical bar construction with four different canisters vertically placed beneath each other. Each of the canisters can be heated independently. For the experiments performed here, only the third canister has been heated. The vertical bar can be inserted in the radiation zone and dependent on the depth of each canister, a different radiation dose will be observed for each canister ranging from 0,45 Gy/h up to 450 Gy/h. The irradiation is performed using ⁶⁰Co sources.

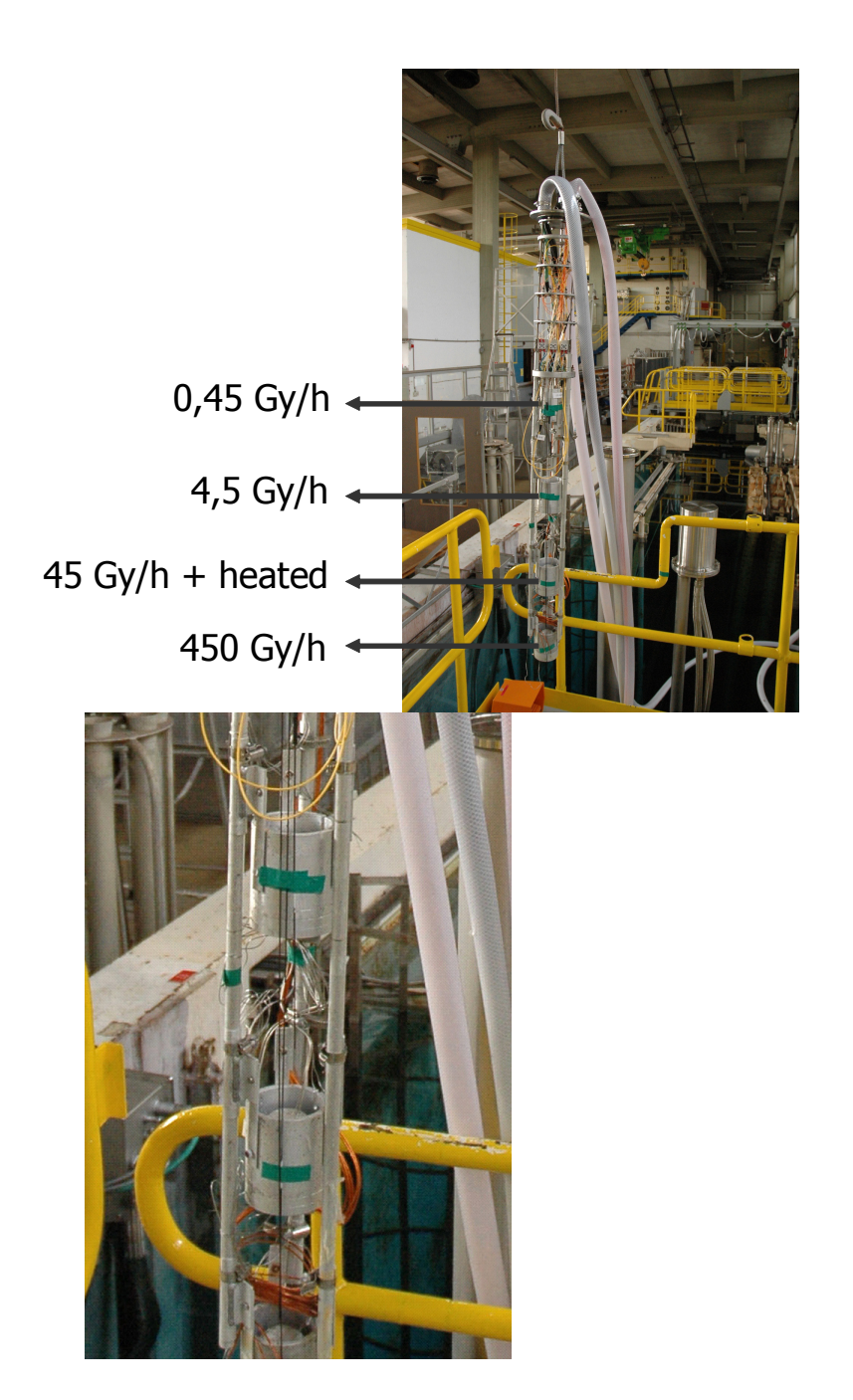


Figure 19: RITA set-up at SCK

Different types of sensors have been irradiated. In total 3 carbon cables according to the specifications of Table 2 have been irradiated as well as 3 tower FBGs without carbon reinforcement but mounted in a capillary tube. Furthermore, also 2 standard FBGs have been irradiated as well: one standard FBG with polyimide recoating in a capillary tube (H₂-loaded fibre/Type I FBG) and one standard FBG with acrylate recoating in a capillary tube (H₂-loaded fibre/Type I FBG). An overview of the different sensors and the radiation conditions is shown in Table 5.

Consequently, in total 8 samples have been irradiated. This has been performed over a total of three radiation periods. Between two subsequent radiation periods, some sensors were changed or removed. Figure 20 shows the temperature variations of the canisters during the three radiation periods as measured with the Pt-100 probes mounted at the side of each

canister. It needs to be mentioned that only the third canister (oven) has been actively heated. However, due to the heat radiation, the temperature of the other canisters was also modified.

During radiation period 2, the Pt-100 probe connected to oven 3 came loose. This caused the temperature readout to drop starting from point G, as shown in Figure 20. But the actual temperature of the oven did not drop. In fact, the oven was further heated because the heating was controlled via the temperature read out of the Pt-100 probe, indicating false readings. Consequently, this also caused a temperature increase in ovens 2 and 4 because of the heat radiation and it explains the temperature rise observed in these ovens. The error was noticed and restored near the end of radiation period 2. In the following, no data points were extracted from the period when the error occurred.

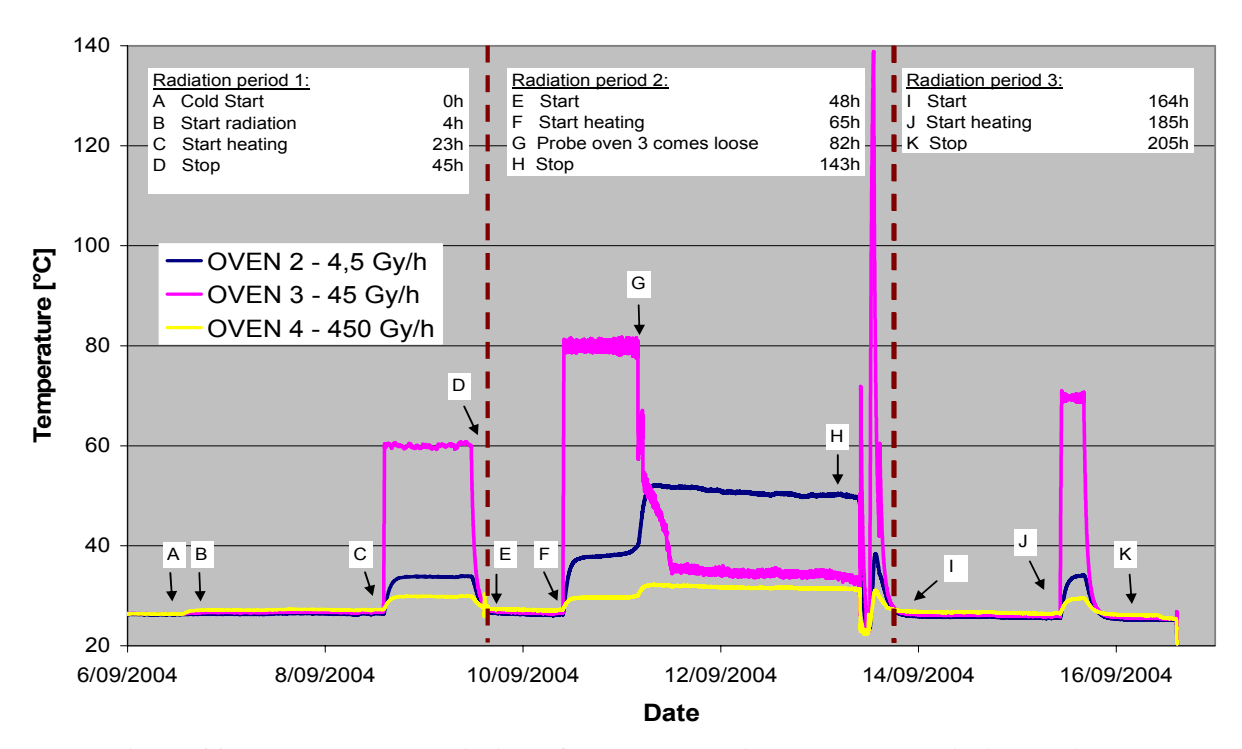


Figure 20: Temperature variation of the ovens during the three radiation periods

| Sensor | Oven | Time | Dose Rate | Total Dose | Period |
|--------------------|------|------|-----------|-------------------|--------|
| | | [h] | [Gy/h] | [Gy] | |
| Carbon cable 1 | 2 | 205 | 4.5 | 923 | 1-3 |
| Tower FBG 1 | 2 | 45 | 4.5 | 203 | 1 |
| Polyimide recoated | 2 | 89 | 4.5 | 401 | 2 |
| Carbon cable 3 | 3 | 205 | 45 | 9225 | 1-3 |
| Tower FBG 2 | 3 | 45 | 45 | 2025 | 1 |
| Acrylate recoated | 3 | 160 | 45 | 7200 | 2-3 |
| Carbon cable 2 | 4 | 205 | 450 | 92250 | 1-3 |
| Tower FBG 3 | 4 | 45 | 450 | 20250 | 1 |

Table 5: Overview of the irradiated samples

As an example, the results of the sensors 'Tower FBG 2' and 'Acrylate recoated' will be described. Sensor 'Tower FBG 2' was placed in oven 3 during radiation period 1 (see Figure 20). It has been irradiated with a dose rate of 45 Gy/h for 45 hours. This results in a total dose of 2025 Gy. After irradiation, a temperature calibration curve has been measured. Figure 21 shows the comparison between the calibration curves measured before and after the radiation experiment. In addition, the wavelengths at the different temperatures measured during the radiation are also indicated. As can be observed, all data points show a similar relation between temperature and wavelength. This indicates that no significant influence of the radiation on the temperature characteristic does exist for this sensor under the above conditions.

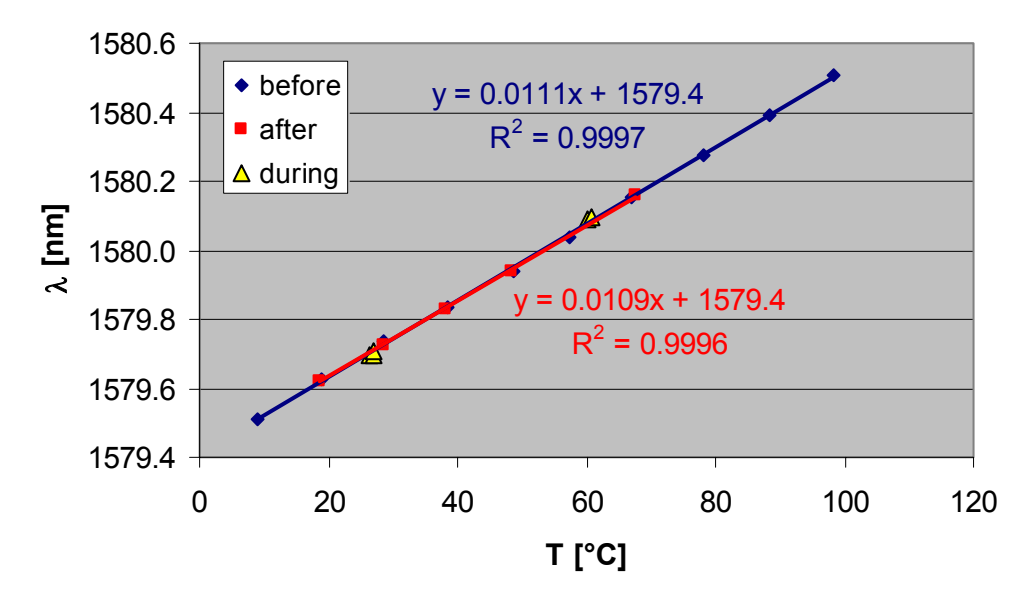


Figure 21: Temperature response of sensor 'Tower FBG 2' before, during and after radiation

The second example, the 'Acrylate recoated' sensor, is an example of a sensor that does show some influence of the exposed radiation. This sensor was placed in oven 3 during radiation periods 2 and 3. It was thus exposed to the same dose rate of 45 Gy/h but now for 160 hours. This results into a total dose of 7200 Gy. Figure 22 shows the comparison between the calibration curves measured before and after the radiation experiment together with the wavelengths measured during the radiation periods. As can be observed, there is a difference in offset between both calibration curves. The slope and hence the temperature sensitivity stays almost unaltered but the absolute wavelengths have shifted with 87 pm, corresponding to a fictitious temperature change of roughly 9 °C.

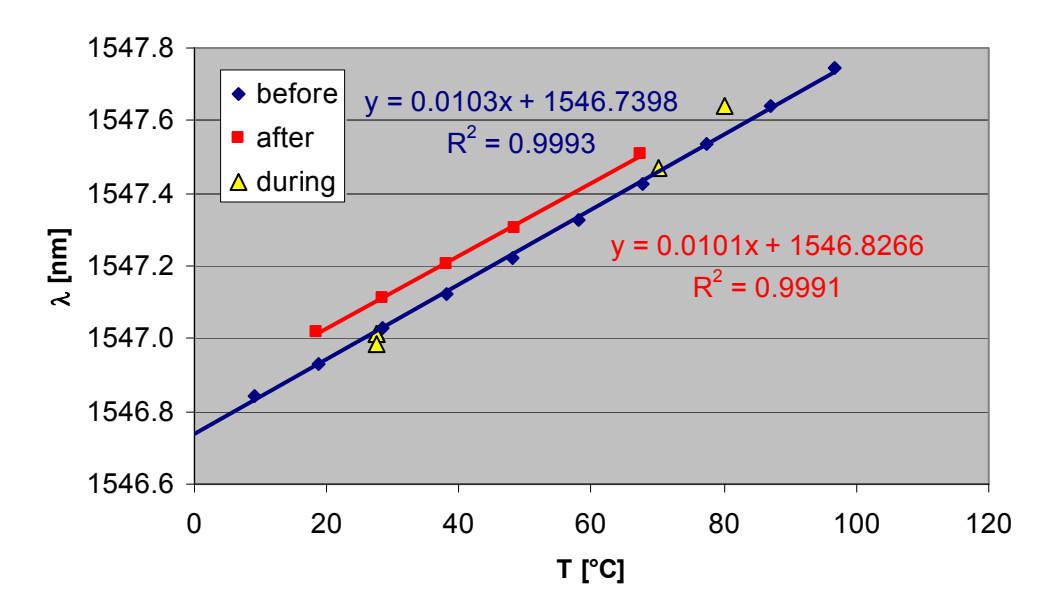


Figure 22: Temperature response of the acrylate recoated sensor before, during and after radiation

In Annex E, the results from all sensor types are presented.

Table 6 gives an overview of the deduced calibration coefficients for all sensors from the calibration data taken before and after the radiation exposure.

| | Ве | efore | | After | Diffe | rence | Absorbed |
|--------------------|----------|-------------|---------|--------------|-----------|----------|----------|
| Sensor | Slope | Offset | Slope | Offset | ∆ Slope | ∆ Offset | Dose |
| | [pm/°C] | [nm] | [pm/°C] | [nm] | [pm/°C] | [pm] | [Gy] |
| Carbon cable 1 | 10.0(1) | 1548.653(7) | 9.7(2) | 1548.666(8) | -0.3(2) | 13(11) | 923 |
| Carbon cable 2 | 9.75(8) | 1529.089(4) | 9.96(7) | 1529.066(3) | 0.2(1) | -22(5) | 92250 |
| Carbon cable 3 | 9.7(1) | 1542.117(6) | 9.8(2) | 1542.116(11) | 0.05(27) | -1(13) | 9225 |
| Tower FBG 1 | 11.11(4) | 1579.378(3) | 11.1(1) | 1579.381(5) | -0.02(12) | 3(6) | 203 |
| Tower FBG 2 | 11.08(6) | 1579.410(4) | 10.9(1) | 1579.415(6) | -0.2(2) | 5(7) | 2025 |
| Tower FBG 3 | 11.04(7) | 1579.502(4) | 10.9(1) | 1579.532(6) | -0.2(1) | 30(7) | 20250 |
| Polyimide recoated | 10.1(1) | 1531.542(6) | 10.2(1) | 1531.540(5) | 0.04(15) | -2(7) | 401 |
| Acrylate recoated | 10.25(9) | 1546.740(5) | 10.1(2) | 1546.827(8) | -0.2(2) | 87(9) | 7200 |

Table 6: Calibration coefficients from the calibration data taken before and after the irradiation experiments. The errors are shown in brackets. The differences in slope, offset and the absorbed doses are also included

It is observed that the temperature sensitivities for all sensors remain fairly unaltered: differences in slope do not differ significantly from 0. The absolute wavelengths (offsets) however show some larger differences in some cases. The difference is only significant in case of carbon cable 2, tower FBG 3 and the acrylate recoated sensor. Some conclusions might be drawn from this. Firstly, note that the shift might be in both directions (negative for carbon cable 2; positive for tower FBG 3 and the acrylate recoated). It is not clear why the carbon cable behaves differently. Possibly, it depends on the carbon surrounding. And secondly, the size of the wavelength difference depends on the type of fibre. The carbon cable seems to be least affected: its difference is lowest although it took the largest dose. Also the tower FBGs seem to feel rather limited influence from the radiation. Wavelength shifts for both types of fibres correspond to fictitious temperature changes of a few degrees Celsius at

maximum. The acrylate recoated sensor on the other hand seems to be much more sensitive to radiation effects: the difference in slope is largest although it received less than 10 times the dose of carbon cable 2. Wavelength shifts correspond to temperature changes of $8-9\,^{\circ}\text{C}$. Possibly, the polyimide recoated sensor shows a similar radiation dependence as the acrylate recoated because of the same method of fabrication (the H_2 -loading) but this can not be extracted from the experimental data because this sensor received a too small radiation dose.

To conclude, one can state that irradiation with large doses does not change the temperature sensitivity of the sensors, but it can induce an absolute wavelength shift which causes errors on the temperature read out. For absolute temperature measurements, these should be accounted for. Errors will be lowest for carbon cables, then for tower FBGs and highest for (acrylate) recoated FBGs.

2.2.3.5 Evaluation interrogator prototype

The relative and absolute wavelength accuracy has been evaluated. This has been performed using Micron Optics temperature stabilized picoWave-Fibre Fabry-Perot Interferometer (FFP-I). The Fibre Fabry-Perot Interferometer is based on a fixed interferometer design with smooth, uniformly spaced transmission peaks. The FFP-I consists of a lensless plane Fabry-Perot interferometer with a single-mode optical fibre waveguide between two highly reflective multilayer mirrors. The FFP-I is manufactured with fibre pigtails so no alignment or mode-matching is required. The distances between the peaks of the here used system is varying between 0,77 and 0,81 nm

The FFP-I is controlled using the picoWave® Controller which utilises a linear proportional integration control feedback loop to maintain the temperature on the TEC (via thermistor feedback) to within $0.01~^{\circ}$ C of the set value. This results into a set of transmission peaks within a relative accuracy of << 1pm. The absolute accuracy is around 2 pm.

The output of the FFP-I has been coupled into the interrogation system. Figure 23 shows the measurement results for different operational temperatures. As can be observed, a good linearity between the applied and measured values can be observed for all temperatures with a correlation factor of 1.000000. Figure 24 shows the calculated error as function of the wavelength. It can be observed that the relative temperature accuracy at one temperature is around 15 pm. The absolute accuracy over the complete temperature range is +/- 15 pm. This corresponds more or less to a temperature accuracy of 1.5 °C.

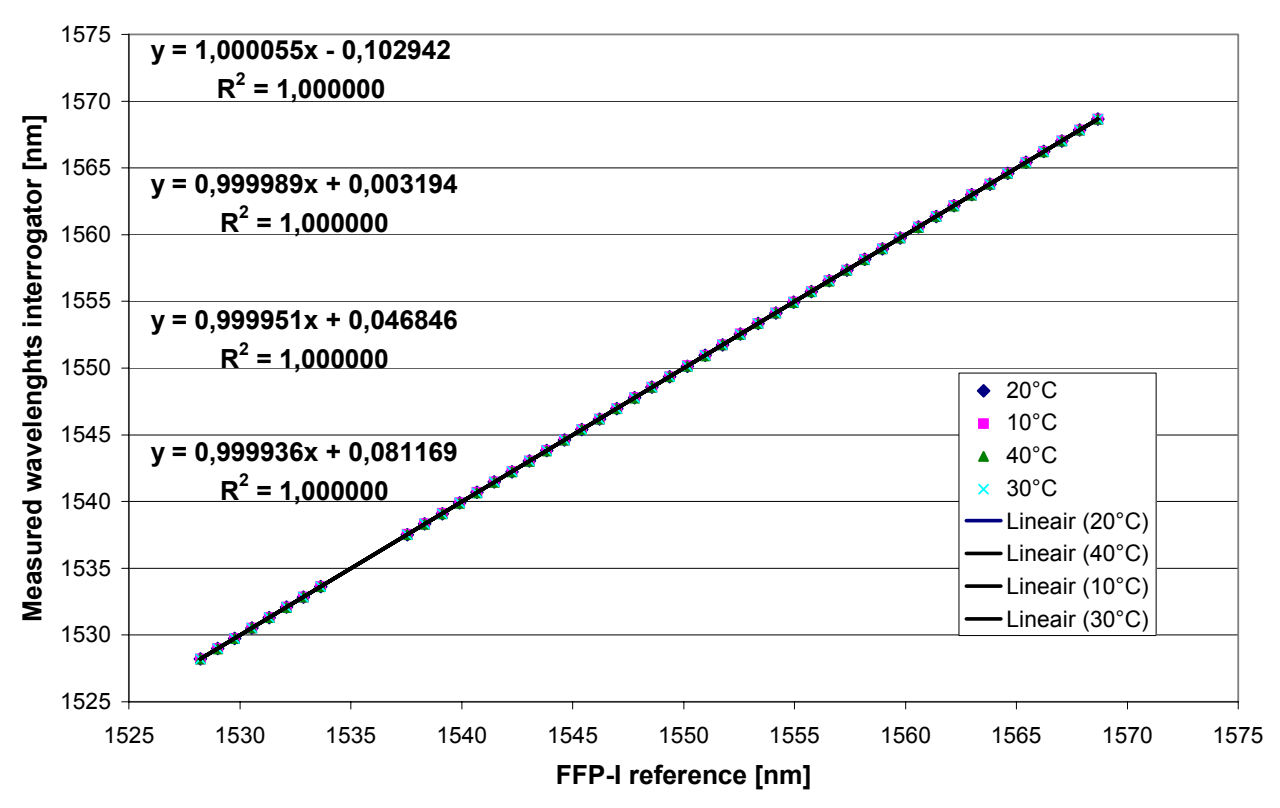


Figure 23: Comparison between transmission peaks of a FFP-I

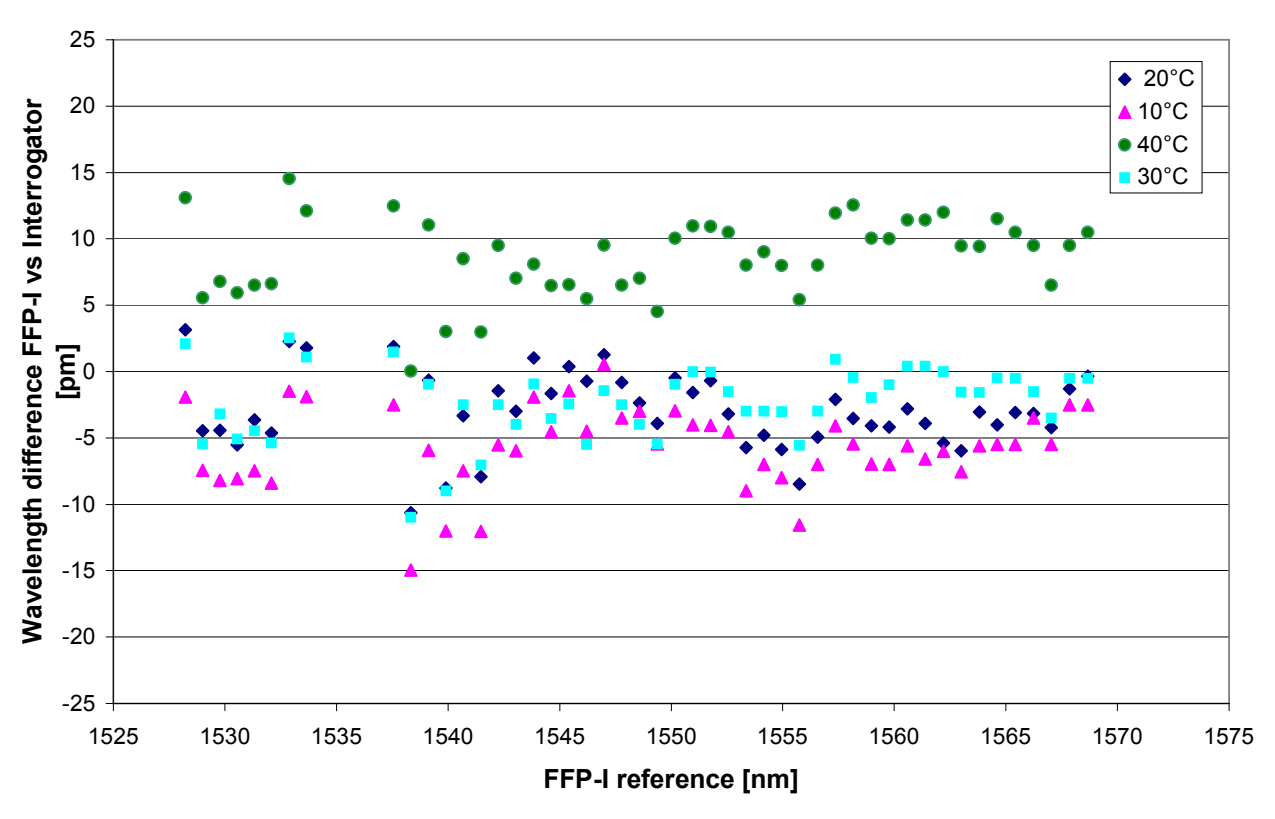


Figure 24: Wavelength error as function of wavelength and temperature

2.2.3.6 Evaluation of the results

Prototypes for sensors and for a sensing system were developed and tested. The newly developed sensors are carbon reinforced tower FBGs. They were found to have good sensor characteristics such as excellent linear dependence on temperature (in the 0-80 °C range) and load (strain). It was found that the carbon reinforcement strongly reduced the strain sensitivity of the FBG-sensors, making them good temperature sensors. The coating also caused the sensors to respond differently on radiation: the induced wavelength shift due to gamma-radiation exposure has opposite sign and is smallest in magnitude compared to bare fibre sensors. From the RITA-experiments, the carbon coated sensors showed the lowest absolute wavelength shift (corresponding to fictitious temperature changes of \sim 2 °C) although they were subject to by far the largest radiation doses.

In the newly developed sensing system, a high power broadband light source (SLED), an 1x8 optical switch, a reference cell and a miniaturised optical spectrum analyser were brought together with the aid of dedicated electronics, housing and software. The system was tested and showed good linearity down to an accuracy of 10 pm. The overall accuracy, taking into account also drifts due to temperature variations, is \pm 15 pm (corresponding to roughly \pm 1.5 °C).

When the above sensors will be used in combination with the above sensing system, temperatures in a radiation environment can be monitored down to an accuracy of a few degrees (1-2 °C shift expected from radiation damage of sensors and 1.5 °C from the accuracy of the sensing system). However, in the next section, it will be shown that the drift due to gamma-radiation levels off in time and therefore the induced error can be corrected for. The accuracy of the measuring system therefore can be further reduced down to the accuracy of the sensing system (1.5 °C).

2.2.4 In-situ installation and operation of a sensing network2.2.4.1 Location of the sensing network

An in-situ test experiment was done at the CORALUS-4 set-up at the SCK in Mol – see Figure 25. In this experiment, several ⁶⁰Co radiation sources are buried in an underground clay layer and the temperature around the source is monitored. Two chains (fibres) of tower FBGs were used for the temperature monitoring. The wavelengths of the different FBG-sensors in the fibres and their positions relative to the fibre start are specified in Table 7.

| | λ | Line 1 | Line 2 |
|--------|------|--------|--------|
| Sensor | [nm] | [m] | [m] |
| FBG-1 | 1530 | 1.50 | 0.50 |
| FBG-2 | 1532 | 3.51 | 2.51 |
| FBG-3 | 1534 | 5.47 | 4.52 |
| FBG-4 | 1536 | 7.47 | 6.53 |
| FBG-5 | 1538 | 7.81 | 6.80 |
| FBG-6 | 1540 | 8.11 | 7.12 |
| FBG-7 | 1542 | 8.40 | 7.41 |
| FBG-8 | 1544 | 8.69 | 7.73 |
| FBG-9 | 1546 | 8.98 | 8.01 |
| FBG-10 | 1548 | 9.27 | 8.30 |
| FBG-11 | 1550 | 9.61 | 8.62 |
| FBG-12 | 1552 | 9.90 | 8.90 |
| FBG-13 | 1554 | 10.20 | 9.22 |
| FBG-14 | 1556 | 10.48 | 9.51 |
| FBG-15 | 1558 | - | 11.51 |

Table 7: The FBG wavelengths and their locations as measured from the beginning of the optical fibres

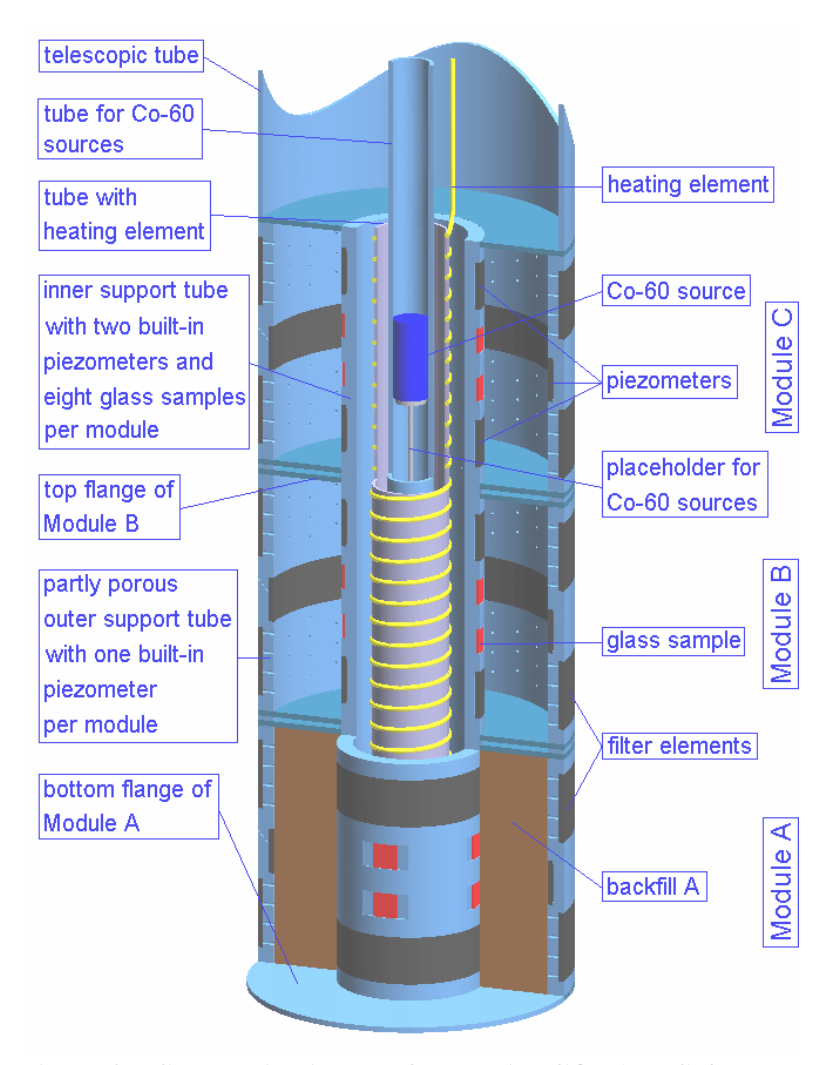


Figure 25: Schematic picture of the entire CORALUS-4 set-up

Before inserting the fibres into the set-up, a temperature calibration was performed in the lab so that the calibration coefficients were known. After the CORALUS-4 experiment, the fibres were removed and another calibration was performed for comparison.

Bare fibre was used instead of carbon coated fibre because the fibres were inserted into 2 mm diameter capillary tubes which made some bends that were sharper than foreseen. The sharp bends prevented the stiffer carbon cables to be inserted. The capillary tubes are located in the part labelled 'Module B' in Figure 25. A schematic picture of the tubing is given in Figure 26. The first line was called 'Module B' and makes three circular loops of 28.9 cm diameter (= 90 cm circumference) around the ⁶⁰Co source and then it goes up again. The second line, called 'REF', is similar to the previous one except that it makes only one circular loop around the radiation source.

The spacing of the gratings of the Module B line was designed in this way that most of the gratings (number 4 to 14) have a close spacing inside the 3 loops. The spacing is 30 cm, corresponding to roughly 3 FBGs per loop. The first 3 gratings have a larger spacing (2 m) and are meant to monitor the temperature in the part preceding the loops, estimated to be roughly 7 m. Similarly, the REF set-up was designed with close spacing between gratings 4 and 14 (30 cm) and large spacing for the first three gratings.

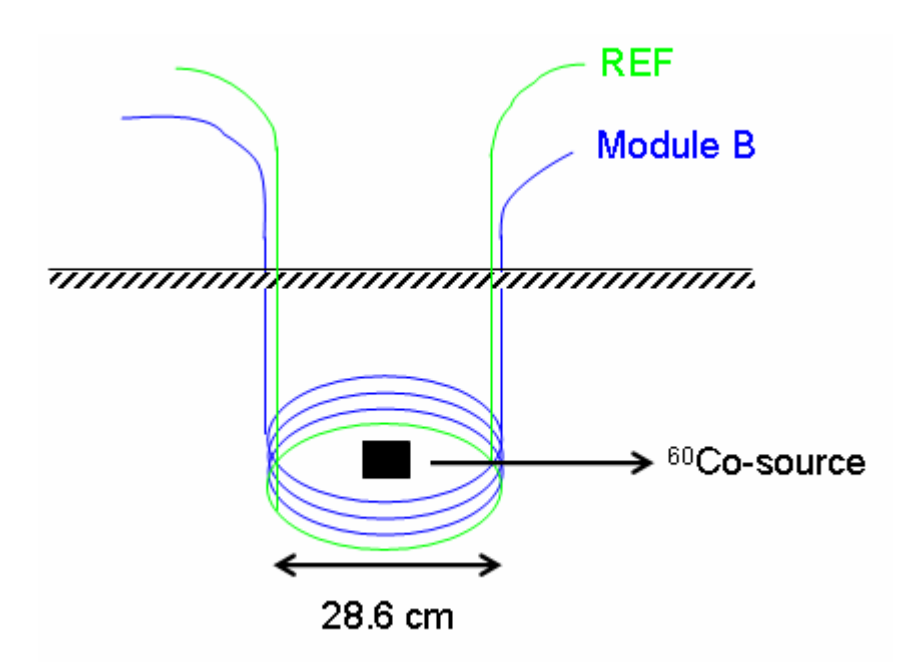


Figure 26: Schematic representation of the measuring lines of the CORALUS-4 set-up



Figure 27: The optic fibres being inserted into the capillary tube using the blow-in method at the CORALUS-4 set-up in the underground laboratory at SCK in Mol

2.2.4.2 Installation of the sensing network

The fibres were inserted into the capillary tubes at the CORALUS-4 test set-up, using the blow-in method, as described in section 2.2.4.2.

Figure 27 shows a picture of the fibre being inserted into the tube. The initial temperature read-outs after installation are presented in Figure 28. The temperature read-out of the sensors in the circular loops is expected to be highest (around 70°C) since the heating element is located close to the radiation source. For the REF line, the loop position seems to be somewhere between FBG-11 and FBG-15 i.e. between 8 and 11 m since temperature is reaching 70 °C here. The distance to the start of the loop thus is slightly more than the estimated 7 m. For Module B, the loop seems to start only near 11 m, since temperature is reaching 70 °C at FBG-14 i.e. at 10.48 m. Hence, there are no sensors actually located inside the 3 loops of this line, as was originally foreseen. Because actual and accurate installation dimensions are lacking, the error can not be "re-calibrated" (it requires the dismantling of the CORALUS experiment with a-posteriori measurements.

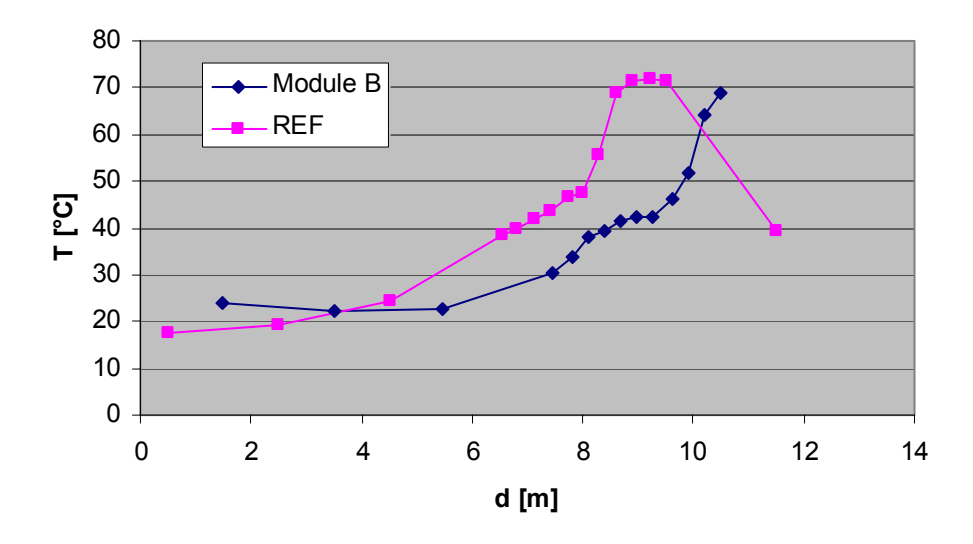


Figure 28: Initial temperatures of the sensors from both lines as a function of position of the sensor in the fibre

2.2.4.3 Operation of the sensing system and comparison with conventional sensors

Both lines were monitored during 42 days after installation of the fibres into the CORALUS-4 set-up. The temperature variations for all sensors were recorded and the relative temperature differences with respect to the initial temperature values are shown in Figure 29 and 30.

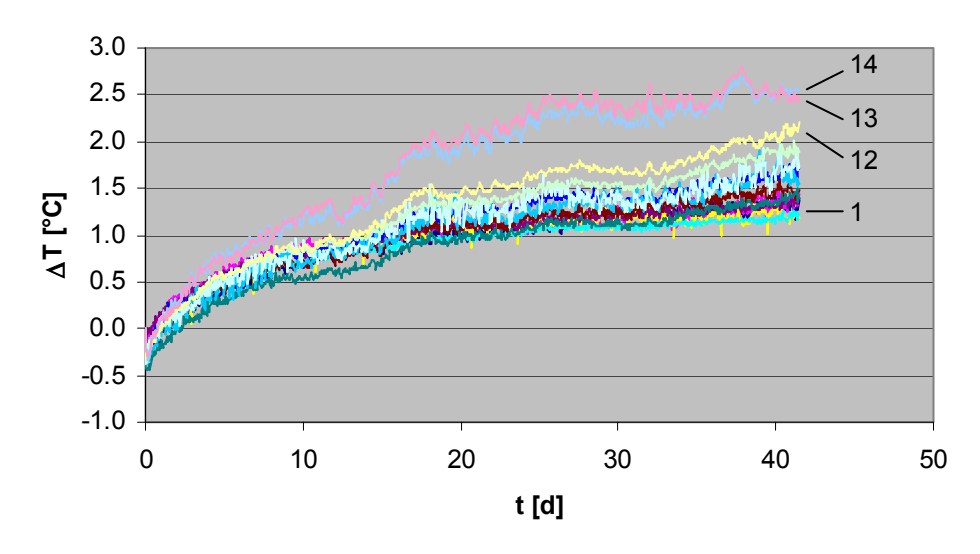


Figure 29: Temperature shift with respect to the initial temperature of the FBG readouts from the Module B line during 42 days

One observes a slight temperature increase for all sensors, which is at minimum 0.5 °C and at maximum 2.5 °C. The shift is largest for FBG-13 and 14 from the Module B line and FBG-13 from the REF line. These 3 gratings were all located close to the radiation source. Therefore, the observed shift is possibly due to the presence of the gamma-radiation. Note that, according to

Table 6, the FBG-wavelength is indeed expected to increase when exposing a naked tower FBG to gamma-radiation. However, care should be taken because the observed shift might equally come from a real increase in temperature.

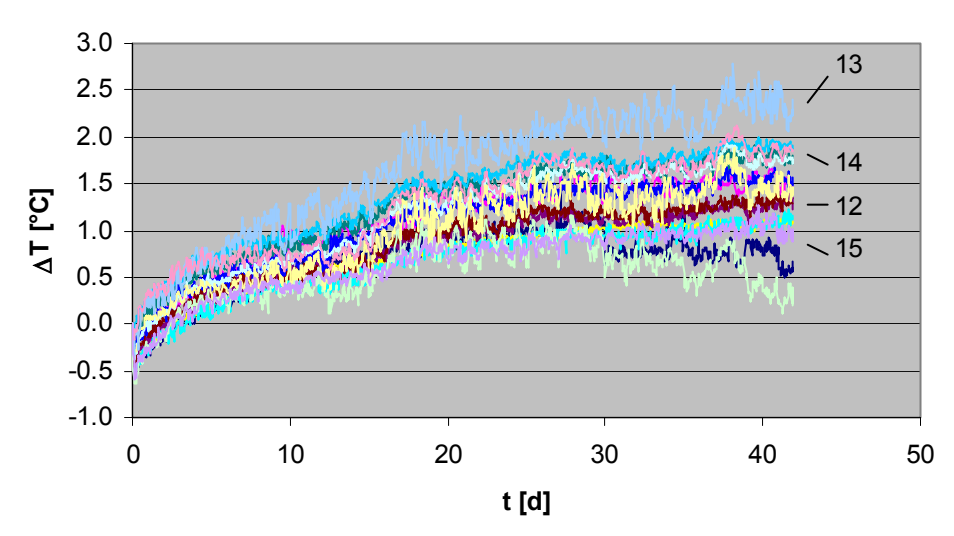


Figure 30: Temperature shift with respect to the initial temperature of the FBG readouts from the REF line during 42 days

To cancel out possible temperature drifts, the FBG-readouts are corrected with the readings from a conventional thermocouple sensor, which is assumed to be immune for radiation. Several thermocouple sensors were used in the CORALUS-4 set-up but only one, called Cor4BTout, was located at the optical fibre loop position. The readout of this thermocouple is presented in Figure 31. One observes an increase in temperature that is almost stepwise but the temperature variation is rather small. Temperature varies for roughly 0.7 °C and this is not enough to account for the observed increase of roughly 2.5 °C.

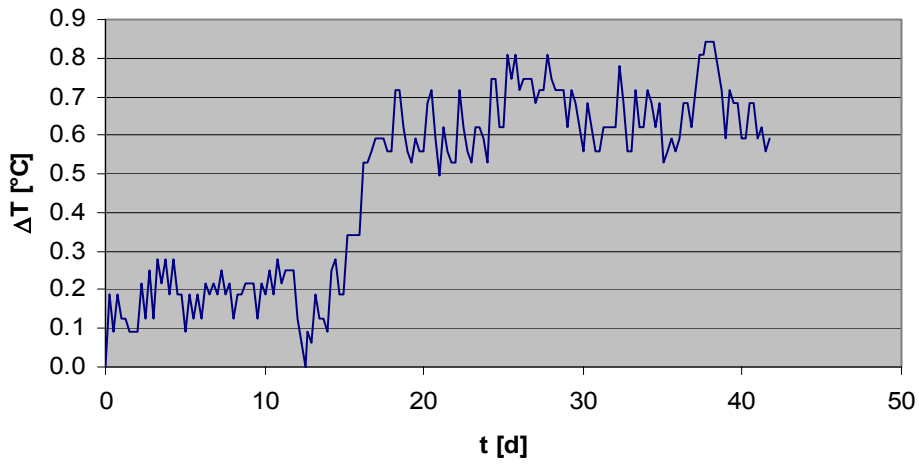


Figure 31: Relative temperature variations of the readout of thermocouple Cor4BTout during the measuring period. This thermocouple was located close to the loops where some of the FBG-sensors were located

The FBG-readouts were corrected with the temperature variations observed with the thermocouple. The results are presented in Figure 32 and Figure 33. The FBG readings now vary for ~ 2 °C at the maximum. Note that this temperature correction only makes sense for the FBG sensors that are located within the loops, i.e. for FBG-13 and 14 from the Module B

line and FBG-11 to 14 from the REF line. This is because the thermocouple was located at the loop positions and the temperature variations at the other sensor positions are unknown.

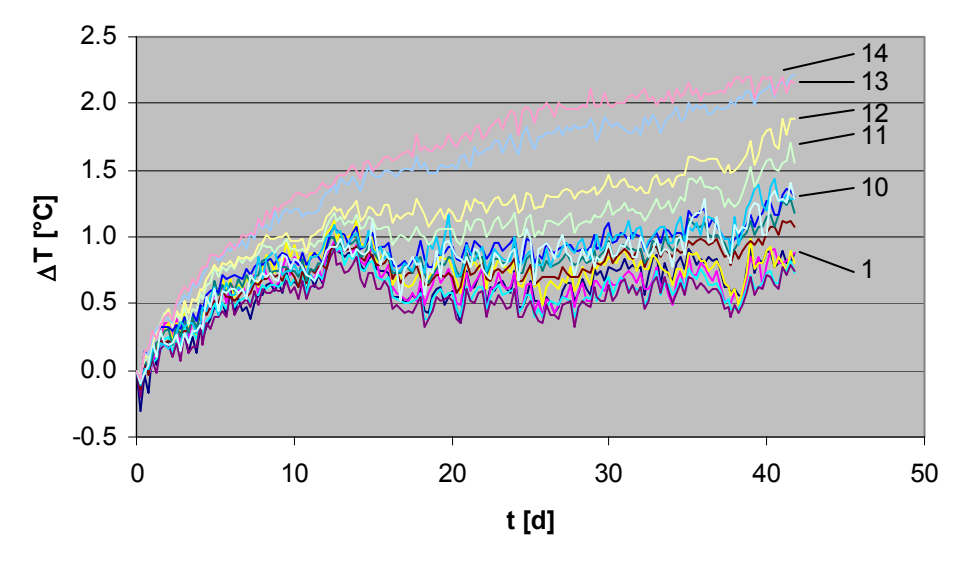


Figure 32: Relative temperature shift of the FBGs from the Module B line, corrected for the effective temperature variations as measured by the thermocouple

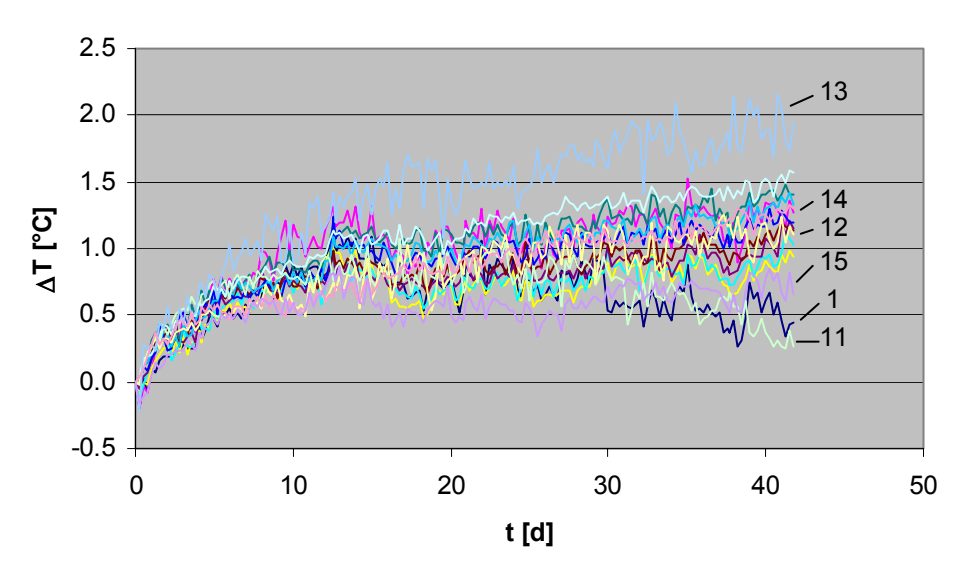


Figure 33: Relative temperature shift of the FBGs from the REF line, corrected for the effective temperature variations as measured by the thermocouple

2.2.4.4 Evaluation of the results

For evaluating the FBG sensors, one can only draw conclusions from the readings from the sensors located in the loop part of the set-up (FBG-13 and 14 from Module B and FBG-11 to 14 from REF) since these sensors were reliably corrected for temperature variations via the readings from the thermocouple. The increase of the other FBG-sensors is probably due to a combination of temperature increase and radiation effects. Note that the first FBG-sensors were not exposed to radiation because they were located in the first part of the tube and therefore behind a lead wall intended for shielding. In particular FBG-1 from the REF line, located at 0.5 m from the start of the tube surely was shielded from the radiation source and therefore should have received a reduced dose. The observed slight increase (0.5 °C) therefore

probably only comes from a slight temperature increase. Note that the scattering on the data is small (< 0.5 °C). This scatter represents the stability of the sensing system.

The radiation effect is best seen in Figure 32 (Module B). The observed increase of sensors 13 and 14 is purely coming from the radiation effect because of the temperature correction. The temperature readout is shifted by ~ 2 °C but the shift seems to stabilise at the end of the measuring period. The other sensors are located further away from the radiation source (see Figure 28) and thus received lower doses of radiation. The shift of the readout of these sensors therefore also goes down when moving further away from the source, as expected.

Figure 33 seems to confirm this picture, although the interpretation is more difficult here. As from Figure 28 one would expect FBG-11 to 14 to be inside the loop part of the tubing, because all 4 sensors give the same absolute temperature of approximately 70 °C. But from Figure 33 and from the previous only FBG-13 seems to be in the loop. A shift of \sim 2°C for this sensor is observed, the same as for the Module B line. The neighbouring sensors, 12 and 14, already show a reduced shift and are therefore probably further away from the radiation source. Possibly, the circumference of the loop was slightly smaller than 90 cm so that only one sensor was inside the loop. The fact that the absolute temperature readout of the neighbouring sensors is the same is because the heating gradient is different than the radiation gradient. The heating system is very homogeneous over the entire distance, while the Co-60 sources are three discrete point sources resulting in a non-uniform distribution.

One can conclude that the radiation exposure at the CORALUS-4 set-up confirms the findings of the RITA-experiment, that is: exposing a naked tower FBG to gamma-radiation causes the wavelength to increase, yielding a fictitious temperature increase. The increase was at maximum around 2 °C (corresponding to roughly 20 pm wavelength shift) and decreases for lower absorbed dose rates i.e. for sensors further away from the radiation source. Furthermore it was observed that the rate of the observed temperature increase was largest in the first part of the measuring period and was stabilizing near the end of the data taking period of approximately 40 days. Therefore, the radiation effect on FBG-sensors settles down and the temperature shift can be corrected for by performing a recalibration once the radiation effect has settled down. This means that the FBG-sensors are still valid candidates for absolute temperature monitoring purposes in nuclear waste repositories.

2.3 Hydrogen detection

2.3.1 Selection of the sensor prototype

The review of the scientific and technique bibliography carried out related to H_2 optical fibre sensors, resulted in the following conclusions: two types of sensors can be developed based on the absorption of the hydrogen in an extrinsic configuration (the fibre is not used as a sensing medium but as a waveguide for the sensing signals) and a third type of sensors can be based on secondary effect of the hydrogen diffusion in the optical fibre itself (intrinsic sensing).

Materials that absorb hydrogen are metals which act as catalytic elements to fix the hydrogen and chemo chromic materials; in both cases the absorption of hydrogen produces changes of the reflectance or transmittance properties of the metal surface. In the case of chemo chromic materials, the changes on reflectance and transmittance are wavelength dependent. The materials susceptible of being used with this purpose are mainly transition metals, which undergo dramatic changes in absorption in the visible or infrared spectrum with the insertion

of electrons and hydrogen, and oxide of the transitions metals and rare earth that the reflectance or transmittance properties change dramatically for some wavelengths and remains constant to the others wavelengths. The main catalytic elements found in the bibliography are Pd (palladium) and Pt (platinum), and as chemo-chromic materials are the oxide of transitions metals as WO_3 (tungsten oxide), V_2O_5 (vanadium oxide) and SnO_2 (tin oxide).

The efforts were focussed on the use of Pd as absorbing element of H_2 in order to be used in both concepts, as an adsorbing material in which the mechanical and optical properties are modified, and a catalytic element to be able to capture the hydrogen close to the chemo chronic material.

Another adsorbing material to use is the optical fibre itself. The SiO₂ molecule is capable to absorbing hydrogen that causes a high change in the transmission properties in the UV region. Furthermore of the UV absorption the hydrogen causes absorptions in the IR region (1 245 nm) that could be easy detected using standard communications optical fibre. The advantage, a priori, to use this type of sensor is the possibility to add long length of fibre in other to obtained the necessary resolution, and then is possible to use non linear effects as the basis for the measurement system.

These concepts have been used in order to start the implementation of first sensors prototypes, based on extrinsic optical fibre sensors, as mirrors, micro-mirrors and thin films metallic elements placed on the end of fibres or on the external plates.

Besides the transmittance or reflectance change produce by the hydrogen in the sensor element, some of the efforts are centred on other concept of sensors. These are based on a fibre Bragg grating (FBG) with Pd coated, in which the hydrogen absorbed by the Pd causes a stress depending of the hydrogen concentration and causes a change in the transmission or reflection spectra of the FBG. This sensor concept has special interest in our case, because allows us to implement a network sensor system with FBG written at different wavelengths, related to different locations. The traditional used of theses sensors as temperature sensor provide too the possibility to eliminate the temperature effect simultaneously with the hydrogen detection.

2.3.2 Construction of prototype sensor

Three sensors prototypes have been undertaken:

<u>PROTOTYPE A: Sensors based on transmission/reflecting properties of semitransparent</u> layers of catalytic elements

A reflection/transmission cell element has been designed for the study of the different samples. The system has been configured in order to be used as a small optical fibre spectrophotometer that connected with the actual laboratories facilities provide information of the reflectance or transmittance changes due to hydrogen absorptions.

The following work is with the prototype designed using Pd/SiO₂ (layer/substrate) mirrors. For thickness of 18 nm of Pd and working on transmission set-up, transmittance changes of 5 % are obtained when levels of 1.5 % concentration of H₂ in N₂ are introduced in the reactor. The sensibility of the sensor is independent of the wavelength in the range from 1200 to 1600

nm, showing similar results in time constant and sensitivity for 1300 and 1550 nm laser light. An important point related to the construction of this sensor is the reversibility. Until 1.5 % concentration of H_2 in N_2 the constructed sensor is reversible and show low hysteresis. The main inconvenience of the present sensor is the difficulty to be wavelength multiplexed, as would be desirable

In order to achieve this sensor the following problems had to be solved: the technique for the deposition of the Pd on the SiO₂ substrate is a sputtering deposition system, that need an appropriate handing of the samples, furthermore, important efforts has been performed for the optimization of the deposition of Pd over SiO₂, helped with systematic studies of Pd thickness using an atomic force microscope (AFM).

The key parameter for improvement of the resolution and the time response of an optrode based on semitransparent thin films elements is the Pd thickness. Theoretical knowledge of the transmittance/reflectance versus Pd thickness and experimental studies performed by AFM has driven us to the calibration of the deposition time of Pd in the sputtering system. The optical measurements and the AFM measurements show a perfect agreement between both techniques.

The following results/stages are achieved:

- A method for the calibration and control of the thickness of the Pd deposited.
- A sensor prototype working until 1.5 % level of hydrogen.
- This sensor shows good reversibility at the levels of H₂ indicated.
- The sensor is sensitive to temperature.
- The sensor is not sensible to the wavelength used
- A systematic study of the relation of Pd thickness and the time constant of the sensor.
- Deposition of chemocromic material in order to getting wavelength selectivity.
- Increasing of H₂ concentration in order to be close the phase change in the PdH system. At higher concentrations we expect changes in the behaviour of the sensor and change in the adherence of the Pd to the substrate.

PROTOTYPE B: Fibre Bragg gratins modified by Pb layers

The second prototype of optrode undertaken is based in a fibre Bragg grating (FBG). The main idea of the present sensor is to take advantage of the influence of the hydrogen absorbed by the Pd that causes stress on the FBG, modifying the reflecting wavelength.

In order to getting a working prototype is necessary to reduce the FBG diameter to values close to 20-30 μm , this reduction enhance the stress produced by the hydrogen adsorption on the Pd. The reduction of the diameter of the FBG has been undertaken etching the grating with HF. For standard telecommunication fibres of 125 μm cladding diameter and after 30 minutes etching with 49 % HF solution, the final diameter achieved is of 25 μm , enough for this propose.

In order to measure the change of the wavelength reflection of the FBG a special measurement system has been designed. Using this system the change of the reflection wavelength of four FBG is measured with respect to the temperature and the etching process. As one of the more interesting results, it is noted that while the temperature change is 12

pm/°C the reflecting wavelength of the FBG change 1 nm in the etching process, and remain constant when the etching process is stopped.

The main difficulty found for the construction of this type of sensor has been the handing of a FBG of 30 μ m cladding diameter. A special plastic structure has been designed to support the grating in the etching process and deposition process too. And extra complication was to set up the rest of optical fibre in the Pd deposition system (the fibre with Pd deposited is very fragile).

The initial results of the sensor show low sensibility and low time constant. An increase of the Pd layer on the FBG is needed for higher sensitivity with a possible increasing of the time constant

The following results are achieved:

- A fibre Bragg grating sensor prototype sensitive until 1.4 % concentration of hydrogen.
- A robust structure for manufacturing this kind of sensors.
- A study of Pd thickness in order to obtain more sensitive sensor.
- A theoretical model will be developing for the stress process on the FBG.
- Study of behaviour of the sensor for higher H₂ concentration.

PROTOTYPE C: Intrinsic optical fibre as H₂ sensor element

In order to use the fibre as sensor element, a special set-up measurement system has been designed adapting the spectral attenuation measurement system being in the Optical Fibres Laboratory with a camera for H_2 . After the fibre has been embedded in H_2 2 % concentration a systematic study of the spectral attenuation of the fibre from 1150 nm to 1640 nm has been made, with the following outputs:

- We identified the 1168 nm, 1197 nm, 1245 nm and 1590 nm as absorptions lines of H₂ in optical fibre in this spectral region.
- A strong IR absorption tail of the 2416 nm absorption line is detected.
- In the 1245 nm absorption, 250 hours are necessary for obtained saturation and others 300 hours for removal of the effect after elimination of the H₂.
- The increment of attenuation is closely related to the H₂ concentration following the equation:

$$\Delta \alpha = \Delta \alpha_0 \{1 - \sum B_n \times \exp[-j_n^2 D(H_2)(T)t_d/b^2\} = CP_{H_2} \{1 - \sum B_n \times \exp[-j_n^2 D(H_2)(T)t_d/b^2\} = C$$

with B_n the nth Bessel function, $D(H_2)$ the diffusion constant of the hydrogen and b the ratio of cladding of the fibre. This equation saturated at $\Delta \alpha (dB/km) \approx C * P_{H_2}$

with $C \approx 8dB/km$ and P the partial pressure of the H₂ (0.02 or 2 %).

- All the absorptions due to H₂ are complete reversible include long IR absorption.
- The absorption and de-sorption of H₂ in the fibre is temperature dependent.
- Others absorptions increasing in 1380 and 1525 nm were observed. The first one is the OH⁻ absorption and is not reversible, the second one are related to C₂H₂ (Acetylene) and has been identified as a possible contamination of the fibre by formation of acetylene in the reactor due to rubbers and glues.

As result of this study we can conclude:

- The 1245-nm line is a good wavelength for be used for testing H₂ concentration. The saturation level of attenuation is proportional to the H₂ concentration and can be used as sensor system.
- At 1315 nm the optical fibre is not sensitive for low level of H₂, and this wavelength could be used as reference wavelength.
- This prototype sensor could be used as distributed sensor with OTDR measurement systems.

2.3.3 Construction of laboratory test system

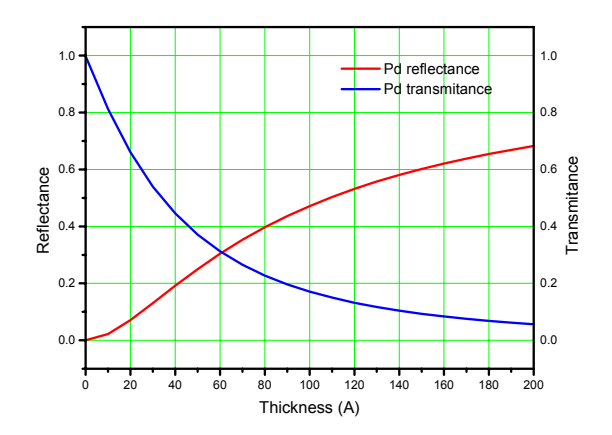
A gas mixture system was designed in order to test sensors in laboratory. The system could handle three sources of H_2 (at different concentrations) and N_2 as main gases as well as other gasses for studying possible interference effects. The entire system is controlled by a computer.

Two chambers (reactors) in which the gas mixture is made, have been designed. The gas chambers have 0.8 l of capacity and all optical and electro optical sensors could be tested.

2.3.4 Test of the sensor or sensor system

PROTOTYPE A: Sensors based on transmission/reflecting properties of semitransparent layers of catalytic elements (Pd)

As explained in previous reports, a reflection/transmission cell element has been designed for the study of the different samples. Prototype A is designed using Pd/SiO2 (layer/substrate) mirrors. For thickness of 18 nm of Pd and working on transmission set-up, transmittance changes of 5 % are obtained when levels of 1.5 % concentration of H₂ in N₂ are introducing in the reactor. The sensitivity of the sensor is independent of the wavelength in the range from 1200 to 1600 nm, showing similar results in time constant and sensitivity for 1300 and 1550 nm laser light. An important point related to the construction of this sensor is the reversibility. Until 1.5 % concentration of H₂ in N₂ the constructed sensor is reversible and show low hysteresis. The main inconvenience of the present sensor is the difficulty to be wavelength multiplexed, as would be desirable.



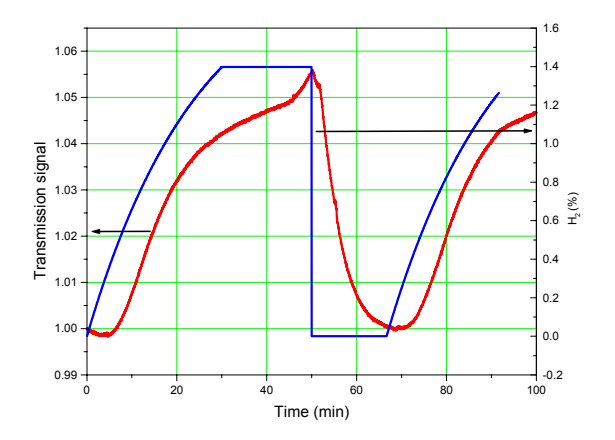


Figure 11a: Theoretical transmittance and reflectance against the thickness for a Pd layer

Figure 11b: Transmittance time dependence of a 18 nm Pd film against the H₂ concentration

PROTOTYPE B: Fibre Bragg gratings modified by Pb layers

The second prototype is based in a fibre Bragg grating (FBG). The main idea of the present sensor is to take advantage of the influence of the hydrogen absorbed by the Pd that cause stress on the FBG, modifying the reflected wavelength.

In order to measure the change of the wavelength reflection of the FBG a special measurement system has been designed. Using this system the change of the reflection wavelength of four FBG with the temperature and with the etching process was measured. As more interesting results, we can emphasize that while the temperature change is 12 pm/°C, the reflecting wavelength of the FBG change 1 nm in the etching process, and remain constant when the etching process is stopped.

The main difficulty found for the construction of this type of sensor has been the handling of a FBG of 30 μ m cladding diameter. A special plastic structure has been designed to support the grating in the etching process and deposition process too. And extra complication was to set-up the rest of optical fibre in the Pd deposition system (the fibre with Pd deposited is very fragile).

A change of the time response of the sensor prototype with respect to the previous results was found. The sensor designed has now a slower time response, mainly in the process of recovery back to initial conditions when the hydrogen is removed. This effect could be due to a Pd ageing process, probably due to superficial oxidation. The Pd, although it is a noble metal that has a great resistance to the oxidation, could suffer a superficial process of oxidation for longer periods, producing a narrow layer (50 Å approx.) of PdO₂. This layer does not block the absorption of hydrogen for the metal bulk, but it produces a delay in diffusion of H₂.

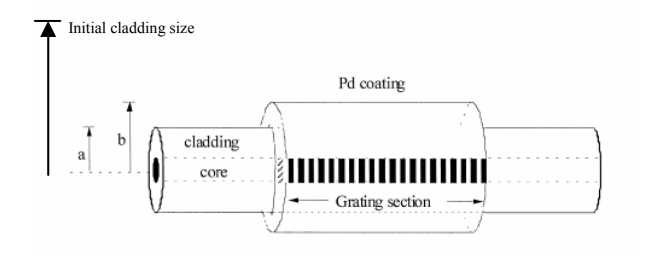
This effect could indicate a reduction of sensor life, however, according to the bibliography, the oxide layer acts like a passivation layer.

Fortunately the sensitivity of the sensor to the H_2 has not changed with the time, staying in 12 pm/ $^{\circ}H_2$, as before. The sensor sensitivity to the polarization of the light has been analysed. The test system designed in the laboratory works with circular light, and then until now, no polarization sensitivity has been observed. However, in a field device the state of polarisation

of the incident light on the sensor can be random. A rotational lineal polarizer was introduced into the system, and the system behaviour for several polarization states was analysed.

The system Pd modified grating shows a change of response for the different polarisations of about 15 pm in the wavelength pick. This polarization sensitivity can be attributed to the rupture of the circular symmetry of the optical fibre due to the etching process or because the deposition of Pd (Pd deposited on only one side of the grating). Fortunately, the wavelength relative change due to the interaction with hydrogen remains constant for all the states polarization tested. In fact the polarization sensitivity of the sensor could be corrected and minimized with an initial calibration for the real polarisation state.

The prototype sensor was also tested for higher H_2 concentration levels. The sensor is able to detect H_2 until 3.5 % concentration, although from the 3 % the sensitivity becomes non-linear with respect to lower concentrations. No degradation in the properties of the sensor has been observed.



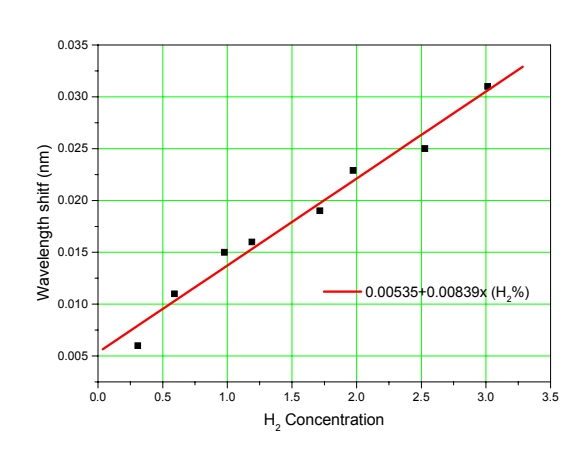


Figure 12a: Schematic diagram of the Pd-coated FBG hydrogen gas sensor

Figure 12b: Wavelength variation of a Pdcoated FBG against H₂ concentration

PROTOTYPE C: Optical fibre as H₂ sensor element (intrinsic sensing)

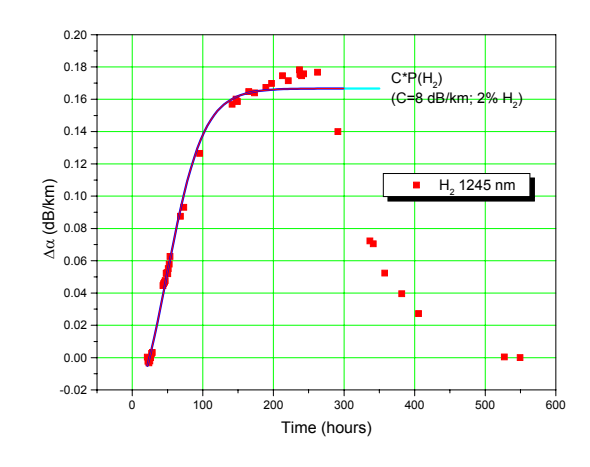


Figure 13a: Time dependence of attenuation coefficient in a fibre for 2 % H_2 concentration at 1245 nm wavelength

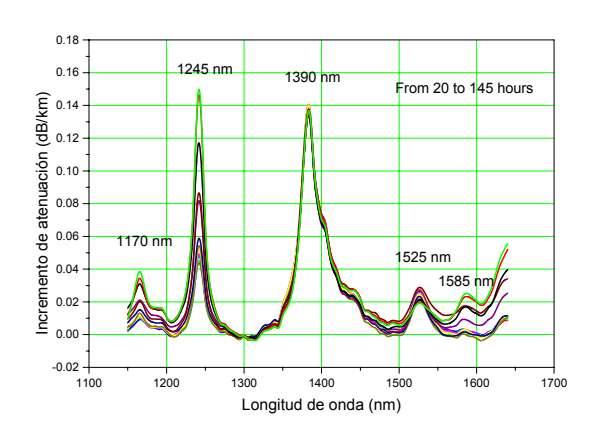


Figure 13b: Absorption coefficient of an optical fibre in 2 % hydrogen

The evaluation of the absorption of H_2 in long length optical fibres has been continued. In new experiments the H_2 concentration was increased from 2 to 4 %. The growth of the attenuation around the hydrogen peaks of the optical fibre is as expected. Additional OTDR measurements have been undertaken in order to know if the diffusion of H_2 in the fibre is a local or bulk processes. The absorption process of H_2 in the 1245 nm absorption is slow: 300 hours are necessary to reach saturation and other 300 hours are necessary to recover to the initial state after elimination of the H_2 . The absorption is produced along the entire fibre and no local effect can be observed in the OTDR measurements. The saturation value of the absorption process for this concentration is slightly higher that the theoretical value.

2.4 Monitoring of radiation

2.4.1 System specifications

The radiation monitoring is based on the radiation induced optical attenuation in optical fibres. This can be done in two ways: integrated by measuring the total attenuation along the fibre sensing path or distributed by employing Optical Time Domain Reflectometry (OTDR).

The requirements for both the radiation sensing and environmental parameters can be summarised as:

- reproducible response for different radiation dose-rates and total doses (no or small hysteresis effects)
- first order transfer function for the relation between optical attenuation and applied radiation dose
- no "photo bleaching" (the injected light does not alter the radiation induced attenuation level)
- low sensitivity with respect to the operating temperature for the case these are unknown parameters (worst case, often temperature is known and can be used for calibration functions)
- high resolution (~ 10 cm) and large dynamic range (~ 60 dBm) for the application of distributed monitoring with OTDR.

2.4.2 Definition and procurement of special doped fibres

Selection of specific doped fibres

Because of the excellent results obtained with the phosphorous-doped fibres in past studies, these fibres are chosen as a primary candidate. Besides the phosphorous doped fibres, erbium-doped and aluminium doped fibres were also considered for the laboratory testing.

The figure below compares the spectral dependence of the radiation sensitivity of the P-doped fibre against pure silica fibres (less sensitive) and Erbium doped fibres (more sensitive).

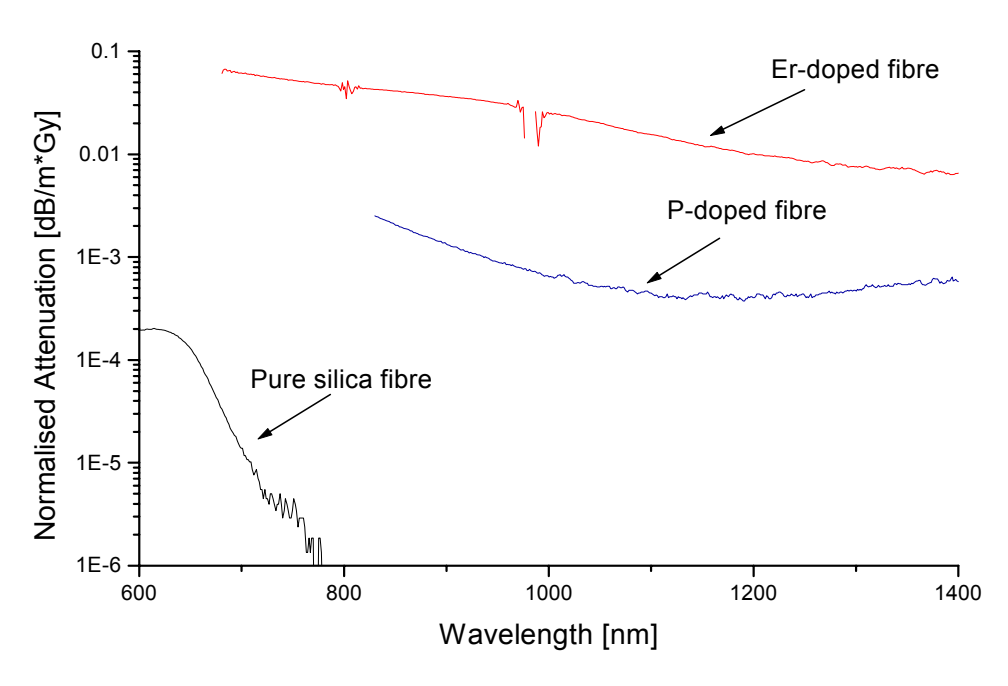


Figure 34: Spectral radiation sensitivity through the dose-normalised optical attenuation for three fibre types (erbium-doped, phosphorous-doped and pure silica fibres)

Fabrication of special fibres

Up to now, no new samples of special fibres have been ordered as the supply of left-over stocks from previous projects is sufficient to carry out the planned experiments. Furthermore, other programmes and projects for studying radiation effects in optical fibres procured sufficient amounts fibre samples. With respect to dosimetry and radiation effects in general, there is a mutual interest between the SOMOS project and internal R&D projects at SCK•CEN.

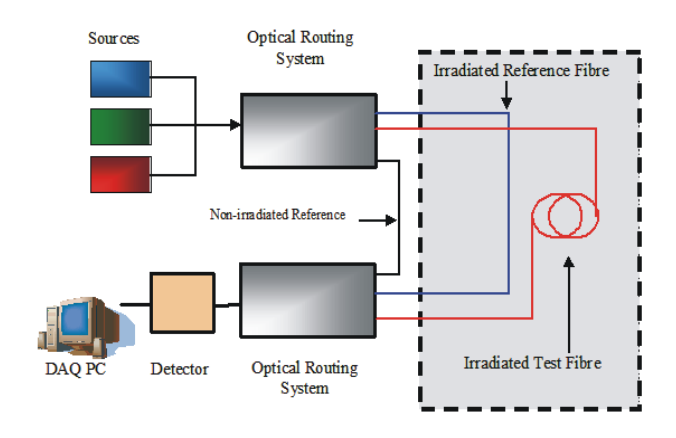
2.4.3 Laboratory testing

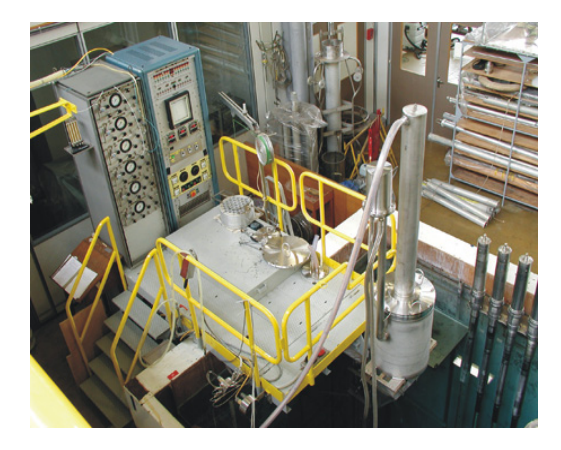
2.4.3.1 Measurement set-up for integrated dosimetry

The phosphorous doped fibres were irradiated in an existing radiation facility which was also used in previous projects on radiation effects on optical fibres. This facility consisted of a matrix of spent fuel elements and a stainless steel "bottle" (in which the fibres and environmental sensors were emplaced). During and after irradiation, the spectral response of the radiation induced attenuation was measured by employing a white light source and an optical spectrum analyser.

Construction of a new irradiation facility

The phosphorous doped fibres were irradiated in more series of irradiation experiments in a new facility with enhanced control of temperature and different dose rates depending on the placement of the fibre samples. The picture below is a schematic of the set-up used





Test set-up used for irradiation P-doped fibres

Picture of the irradiation facility with Co-60 sources

2.4.3.2 Distributed sensing

In an early phase of the project, several commercial vendors of high-resolution OTDR systems were contacted for the potential purchase and one test system was delivered for presales evaluation during two weeks. The tests performed with this system were disappointing: the specifications stated were only reached in terms of resolution and the dynamic range at the same time. High resolution only appears to be feasible with a very small dynamic range (insufficient for the application of dosimetry) or the spatial resolution was well above the requirements (~ 10 cm) to reach sufficient dynamic range. The purchase of such a system was therefore delayed as the high price could not justify the merits for the SOMOS project (and other R&D in the field of radiation effects on optical fibres).

However, by the end of the SOMOS project, new tests with a prototype from Luciol instruments (Switzerland) showed promising results with respect to the required specifications:

- One point spatial resolution < 5 mm
- Two point spatial resultion < 10 cm (this is critical for use in dosimetry)
- Sensitivity of 110 dBm (important for noise thresholds, a common problem in classical OTDR's and optical spectrum analysers)
- Dynamic range > 35 dB (crucial as the online measurements must accommodate a large range of radiation indiuced attenuation changes)
- Optimised for our fibre samples (this is done as the instrument is built according to our requirements).

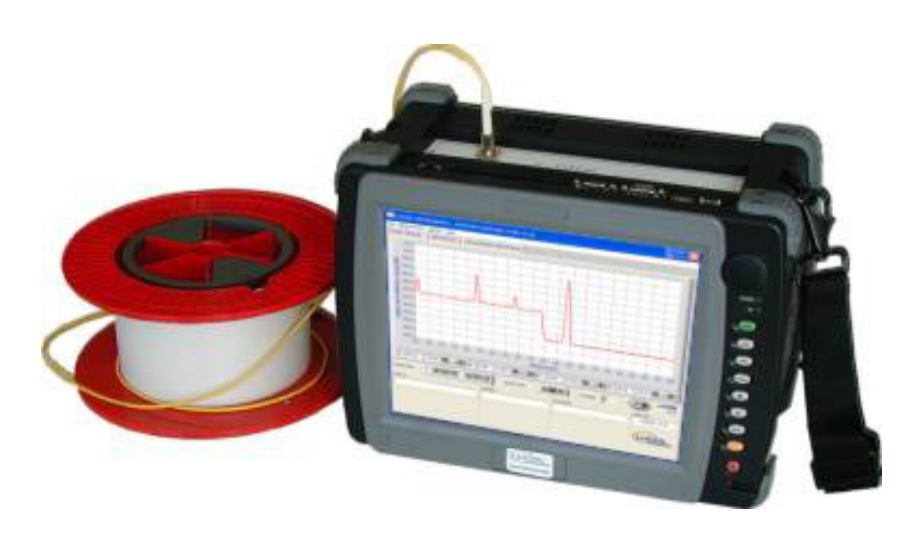


Figure 35: The high-resolution photon-counting OTDR from Luciol

In view of these developments, a purchase was negotiated with Luciol based on our specifications (including integration with existing data-acquisition systems running on LabView). We also obtained a substantial reduction on the normal purchase price as a demonstration unit was to be used as the base (but modified to comply with our requirements). The initial time-frame was foreseen with a delivery during December 2003, but last moment safety compliance requirements shifted that date towards February 2004.

New tests however were again disappointing (not reproducible), in spite of the promising specifications. Even though this does not mean distributed sensing is impossible, the time frame left and available resources were too limited to pursue better results for the SOMOS project.

2.4.3.3 More irradiation campaigns for integrated dose measurements

An initial set irradiation campaigns has been carried out with phosphorous doped fibres at elevated temperatures (with respect to the available data from previous projects which will be partly re-used). Because of a delay in the construction of the new facility, a series of irradiation experiments on the doped fibre samples at different dose-rates, temperatures and total doses was carried out in a preliminary constructed irradiation system at the BR2 facility.

Temperature dependence

The figure below shows a typical result where on-line measurements reveal the robustness of the radiation induced attenuations around 1550 nm of the phosphorous-doped fibres against temperature changes.

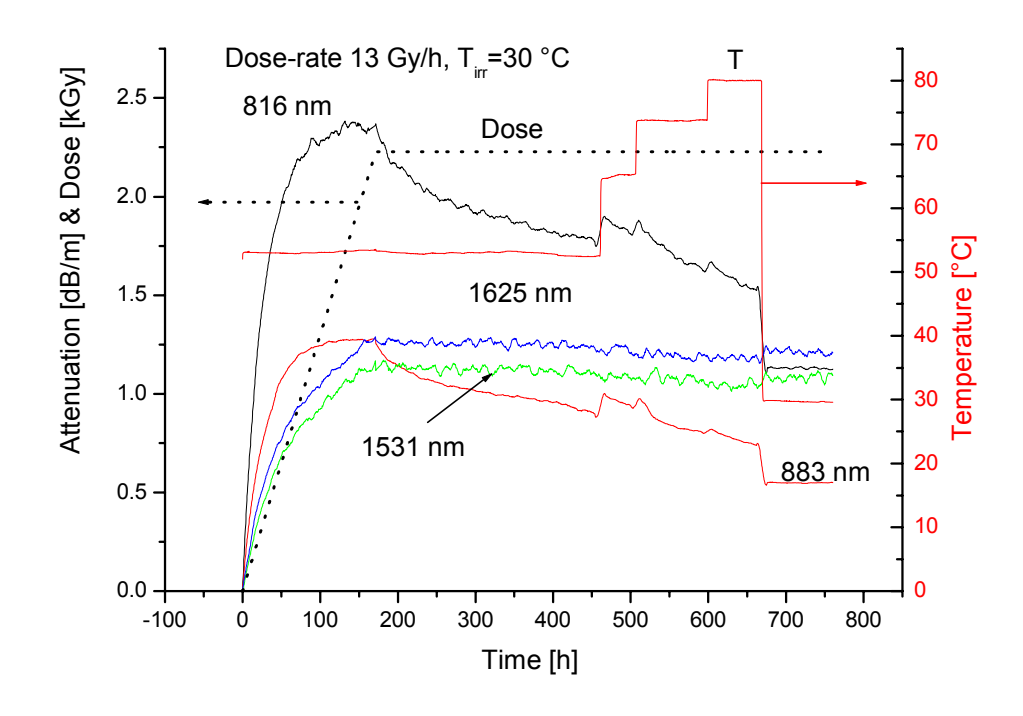


Figure 36: Low annealing (fading) of the attenuation in P-doped fibres around 1550 nm, even with large temperature variations

Dose-rate dependence

Results included irradiations campaigns to investigate the dose-rate dependence. In general, the dose-rate dependence is that the sensitivity to total dose increases with lower dose rates. A practical usability range however is obtained between 1 and 100 Gy/h where the dose-rate dependence proved to be minimal as shown in the figure below.

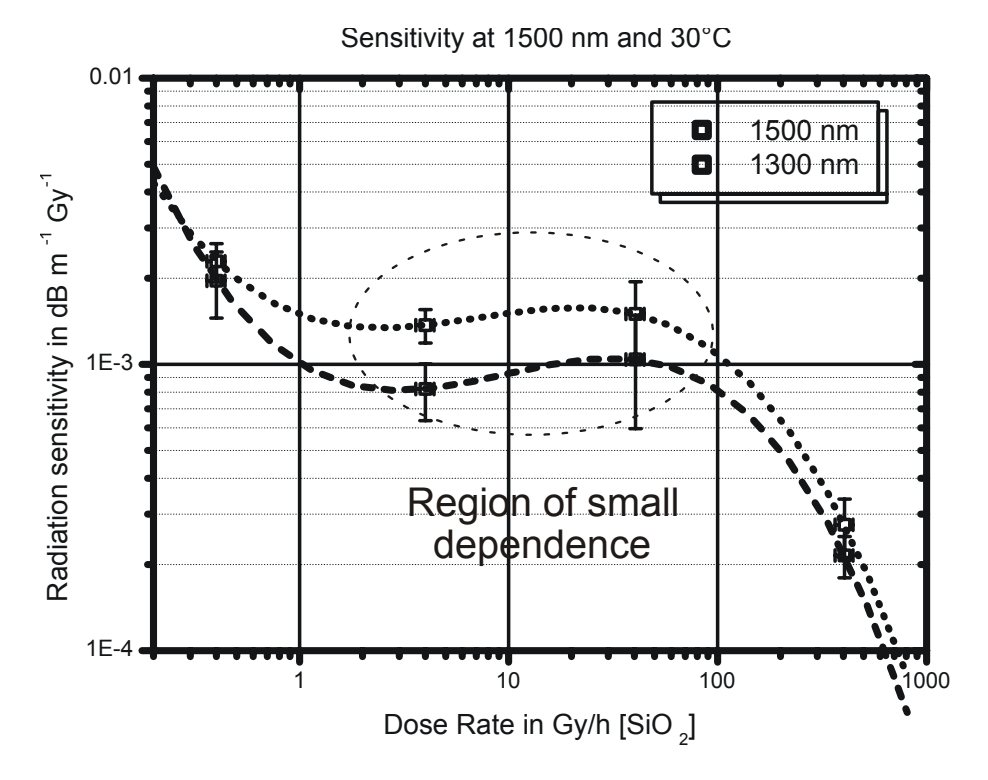


Figure 37: Dose-rate dependence

2.4.4 Prototype design of dosimetric system

The set-up for irradiations in the available facilities was used as a prototype system since also temperature could be controlled.

The dose reconstruction is illustrated below for low and high total doses. Relatively simple calibration curves were obtained for the different dose regimes.

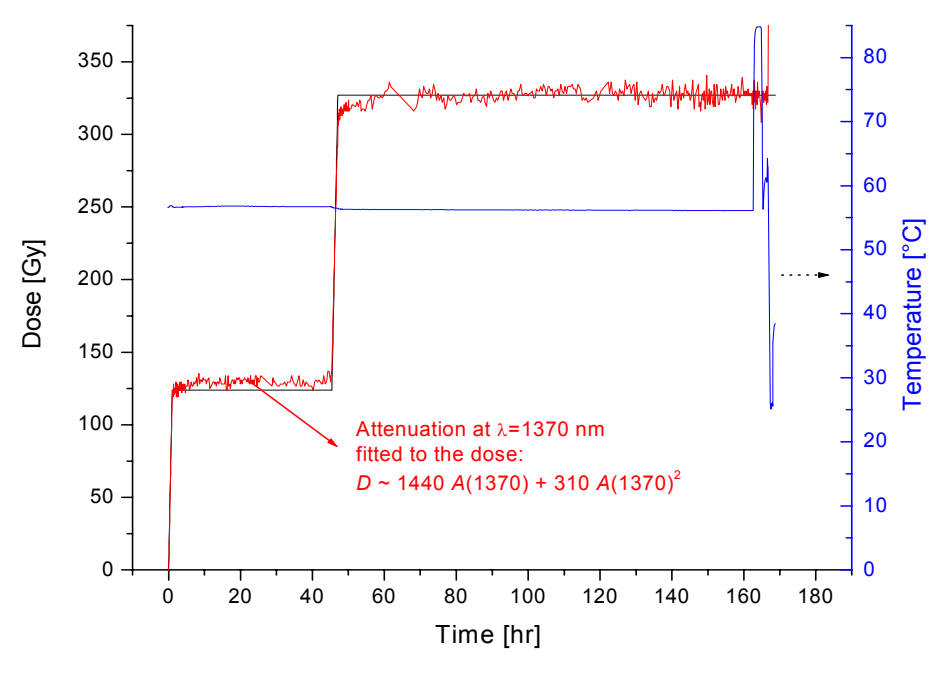


Figure 38: Dose reconstruction for low total doses for two consecutive irradiations. The response can be modelled by a second-degree polynomial calibration function. Note the robustness for post-irradiation temperature variations

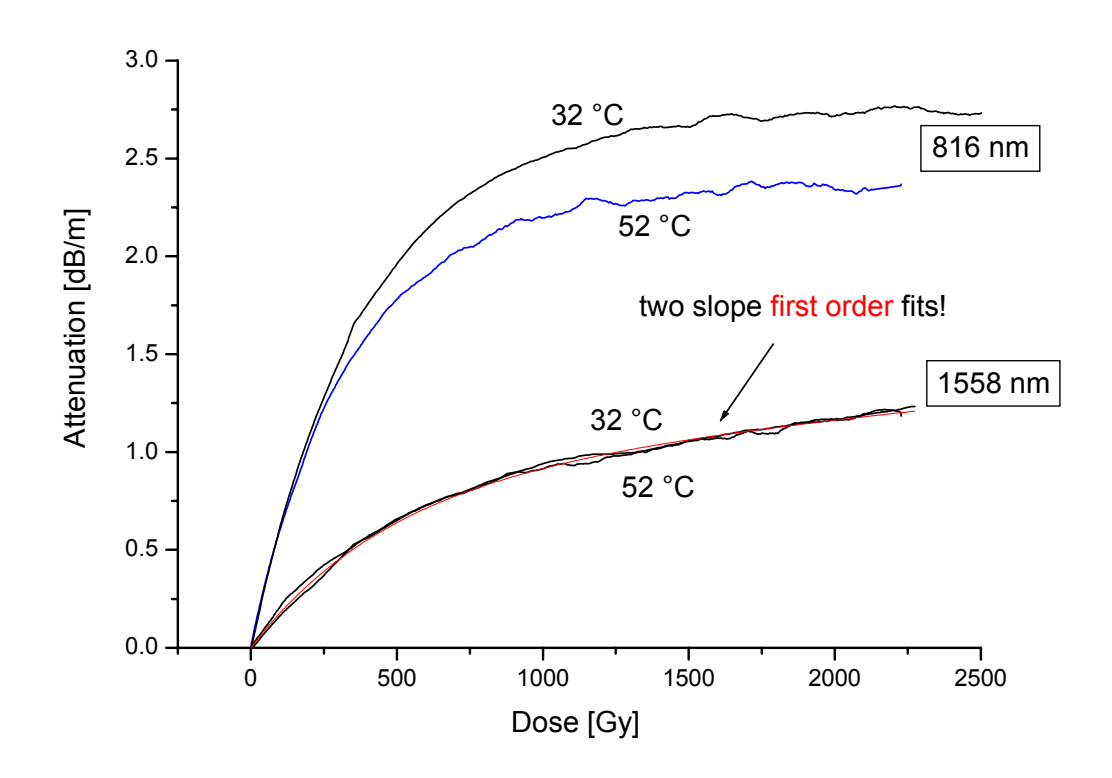


Figure 39: Response for higher total doses at two different temperature regimes during irradiation. The optical attenuation at 1 558 nm is fitted with a two-slope function: the sum of a linear term and a saturating exponential one

2.4.5 In-situ integration

The operational constraints (dust, humidity) of installation in underground facilities are to be taken into account by providing the necessary shielding which is obtained in a similar way for other sensitive instrumentation. The capillary tubes of stainless steel are already emplaced with the CORALUS II experiment in the HADES underground laboratory.

For in-situ integration, a system has been build in order to insert the radiation dosimetry fibre inside the 2mm stainless steel tubes. The system that has been envisaged is an air pressurised system that blows the fibre inside the stainless steel capillary. Preliminary tests have been performed on a laboratory set-up with the same type of capillary as from the CORALUS set-up, see section 2.2.4.1. Figure 40 shows the demonstration set-up. The system exists of a compressor providing pressures up to 10 bar and a fibre insertion tool, shown below. In order to reduce the friction between the fibre and capillary, graphite powder is also blown inside the capillary. The system allows inserting the fibre inside the tubing. It needs however to be noticed that some manual handling still is required but the fibre easily gets installed using this set-up. This method was then also applied in the CORALUS set-up for inserting the temperature sensing cable (carbon re-enforced) into the capillary tubes. While the installation went without any noticeable difficulties for the temperature sensing fibres, the fragile radiation sensing fibres could not be installed fully, making measurements impossible.



Figure 40: Air-pressured fibre blow-in system



Figure 41: Fibre injection system

3 Assessment of results and conclusions

Temperature sensing

For temperature sensing, the focus was on the design and testing of carbon reinforced Tower gratings as in the first part of the project, it could be concluded that the Tower gratings show the least sensitivity under radiation. The carbon coating results in a stiffer but mechanically more durable fibre, whereas classical fibre Bragg gratings are quite fragile. Furthermore, the interrogation system for a distributed temperature sensing network was developed, including dedicated data-acquisition software.

Hydrogen sensing

For hydrogen sensing, three prototypes have been designed, developed and tested in the presence of varying hydrogen concentrations. A first prototype was based on the change in reflection coefficient of a palladium coated mirror. A second prototype employed fibre Bragg gratings where the swelling of a palladium coating due to hydrogen absorption causes mechanical stresses which modify the characteristic wavelength of the Bragg grating. The third prototype employed the characteristic absorption peaks of hydrogen present in the fibre core. In the presence of hydrogen, a part of the hydrogen slowly diffuses into the fibre causing the absorption peak to increase in value. For all three prototypes of hydrogen sensors, adequate sensitivity and reversibility of the process were demonstrated.

Radiation sensing

Radiation sensing is performed through special doped fibres which show a first order (or even linear) increase of the radiation induced optical attenuation around 1300 nm to 1500 nm when placed in a radiation field. The temperature dependence of the response is negligible in the envisaged operating range (20 to 90 °C), while the dose-rate dependence was demonstrated to be low in a region between 1 and 100 Gy/h.

In order to obtain distributed radiation sensing, the use of a high-resolution Optical Time Domain Reflectometer (OTDR) was attempted. Although the specifications, such as a high spatial resolution, high sensitivity and dynamic range seemed to be ideal for distributed

measurements, results obtained were disappointing. Finally, distributed radiation sensing was abandoned for this project, mainly due to resource and time constraints at the end of the project.

In-situ integration

As part of the demonstration aspects of the SOMOS project, temperature and radiation sensing were planned using dedicated stainless steel tubes engineered and emplaced within the CORALUS tests in the HADES underground research laboratory, in Belgium. Though the placement of optical fibres in capillary tubes is a mature technology in telecommunication systems, the particular set-up used is far more demanding. Mainly the fact that the capillary tubes were placed with several loops around the CORALUS test tubes imposed a lot more friction during emplacement. The (fragile) optical fibres used for radiation sensing proved to be impossible to inject fully given the local geometry of the CORALUS experiment, however, the carbon reinforced tower grating fibres for temperature sensing were successfully emplaced and benchmarked against the available classical temperature sensors.

Assessment of the applicability of the monitoring systems in nuclear waste repositories

Of the three sensing techniques investigated, the applicability of a distributed temperature monitoring system using fibre Bragg gratings is well demonstrated. The fact that these fibres can be installed and replaced at all times also guarantees the long-term usability, a property which differentiates this type of systems with classical sensors which can not be replaced after emplacement of waste forms (or it would be very costly to do so). The same advantage is in principle also valid for radiation sensing. Even though the demonstration failed in the in-situ integration tests, a careful design taking into account geometry constraints with placement of the capillary tubes should enable a successful deployment. For hydrogen sensing, where the qualification was valid in absence of radiation, the resulting monitoring system can at least be applied in areas of low radiation inside the repository. In any case, the results of this project should be considered in the overall design of possible monitoring systems for nuclear waste repositories.

4 References

Dr Javier Gutierrez Monreal: "Sensores de fibra óptica para hidrógeno", in workshop "PILAS DE COMBUSTIBLE: Una altenativa limpia y eficiente a las fuentes de energía convencionales", Jaca (Huesca, Spain), 9-11 2002

Dr Javier Gutierrez Monreal: "Microsistemas de gases y micropilas", at the same meeting in Jaca

Dr Pedro Corredera Guillén: "Desarrollo de sensors de hidrógeno basados en fibra óptica", in second workshop "PILAS DE COMBUSTIBLE", Benidorm (Alicante, Spain), 17 September 2003

"Development of Fibre-optic Hydrogen Sensors for Testing Nuclear Waste Repositories" – poster, Seventh European Conference on Optical Chemical Sensors and Biosensors (EUROPT(R)ODE VII), Faculty of Medicine, Complutense University, Madrid, Spain, 4-7 April 2004

- P. Borgermans, B. Brichard, G. Volckaert, J. Vlekken, P. Corredera, J. Gutierrez, M. Aleixandre and M. L. Hernanz: "SOMOS: Safety and Operational Monitoring of Nuclear Waste Repositories with Fibre-optic Sensing Systems" poster and proceedings of Euradwaste 2004, Luxembourg, 29-31 March 2004
- B. Brichard, A. F. Fernandez, H. Ooms, P. Borgermans, F. Berghmans: "True dose-rate enhancement effect in phosphorous-doped fibre-optic radiation sensors", 2nd European Workshop on Optical Fibre Sensors, Proceedings of SPIE, Vol. 5502, 2004, June 2004, pp. 184-187
- B. Brichard, A. F. Fernandez, H. Ooms, P. Borgermans, F. Berghmans: "True dose-rate enhancement effect in phosphorous-doped fibre-optic radiation sensors" poster presentation at EWOFS 2004, 9-11 June 2004, Santander, Spain

5 Contacts

J. Vlekken and M. Voet FOS&S, I.D.FOS Cipalstraat 12 B-2440 Geel Tel. +32-14-581191 Fax +32-14-591514

Web: http://www.fos-s.be

P. Corredera Guillén and J. Guttierrez CSIC/IFA Calle Serano 117

E-28006 Madrid Tel. +34 91 561 8806

Fax +34 91 411 7651

Web: http://www.ifa.csic.es

web. http://www.na.csic.es

G. Volckaert and P. Borgermans SCK•CEN, Dept. WD Boeretang 200 B-2400 Mol

Tel. +32-14-333229 Fax +32-14-323553

Web: http://www.sckcen.be

APPENDIX: Distributed fibre-optic sensing systems

Distributed temperature sensing using the Brillouin effect

Fundamentals of Brillouin scattering

The SBS system is based on the measurement of the Brillouin scattering characteristics. Brillouin scattering is a natural scattering process associated to the propagation of light in a medium like an optical fibre. Due to the interaction of light with the propagation medium different scattering components are generated: Rayleigh, Brillouin and Raman component (see Figure 42). The Brillouin interaction results in the generation of scattered light (Brillouin component) which shows a frequency shift compared to the light causing the interaction. This shift can be attributed to the presence of inhomogeneities associated to acoustic waves in the silica (acoustic phonons).

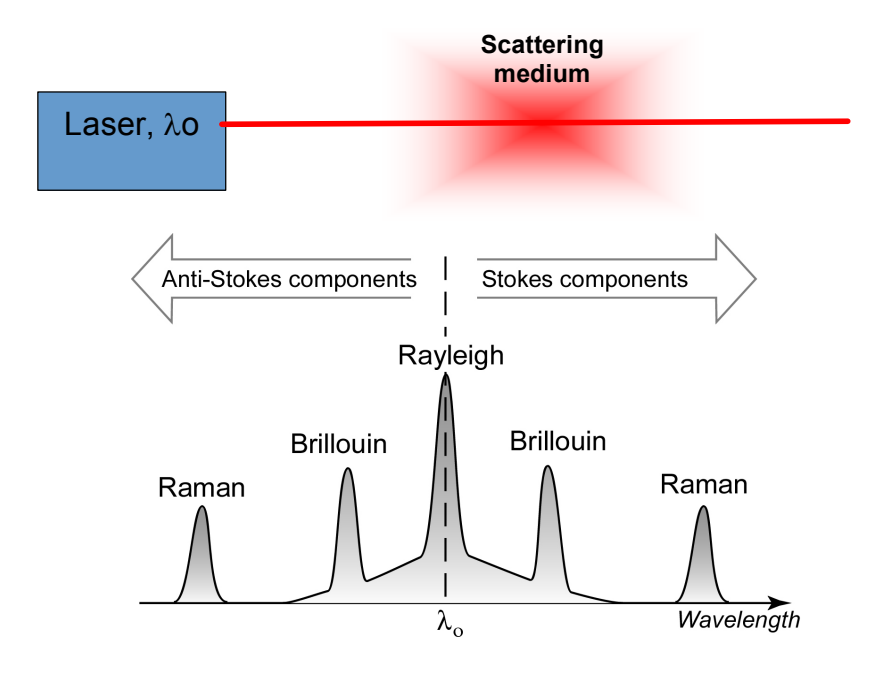


Figure 42: Scattering components in optical fibre

A system based on the analysis of the Brillouin-scattered light in optical fibres is naturally devoted to perform strain and temperature measurement. This can be achieved since the Brillouin shift depends on the acoustic velocity of the medium, which is temperature and strain dependent: The frequency shift depends linearly on the fibre strain and temperature, see Figure 43 and

Figure 44. As a consequence, the scattered light has a slightly different wavelength than the original light and the departure from the original wavelength is directly dependent on the strain and temperature of the fibre.

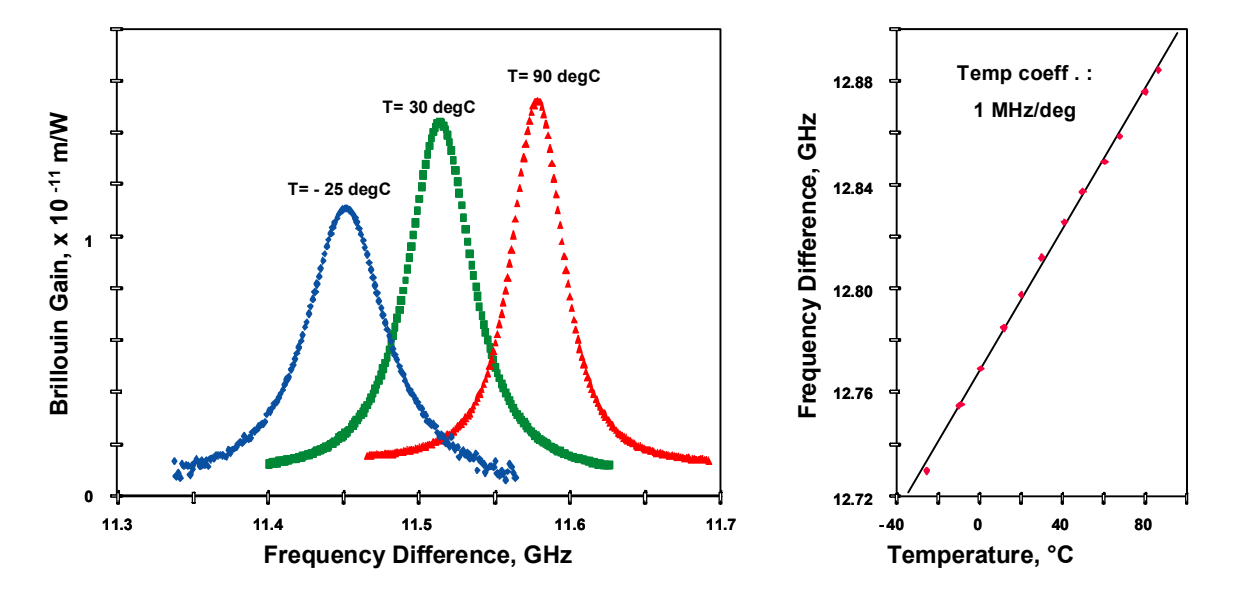


Figure 43: Temperature effects on the Brillouin-scattered components

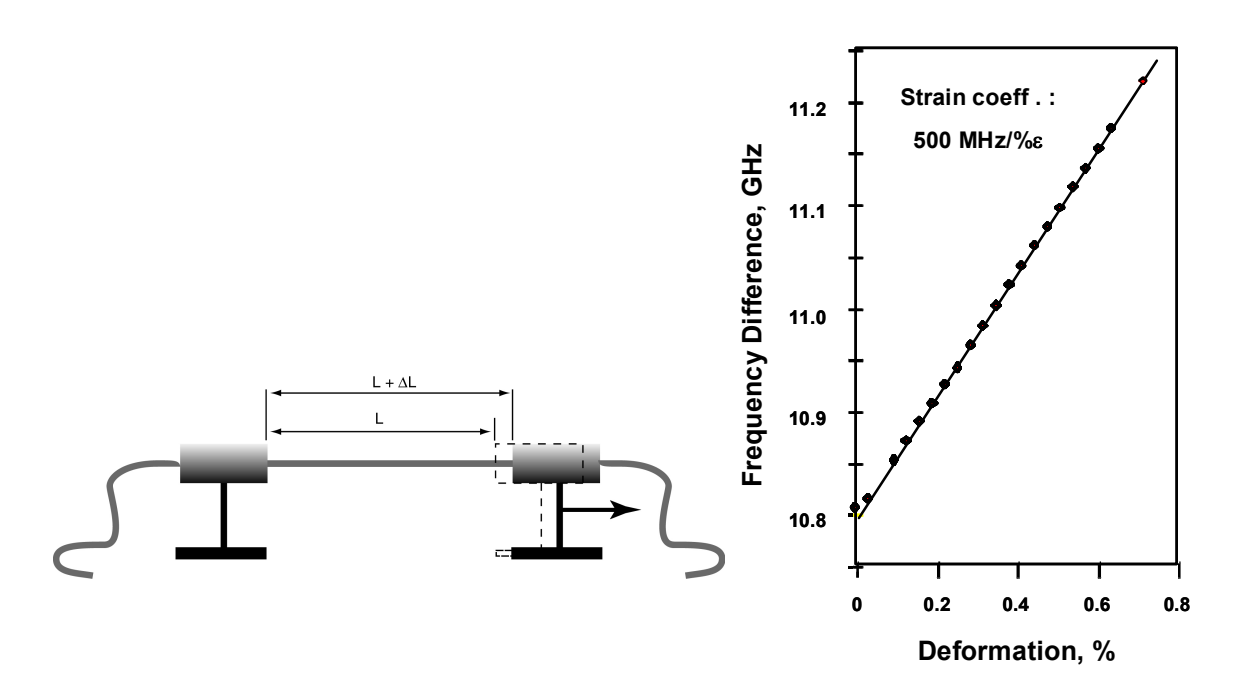


Figure 44: Strain effects on the Brillouin-scattered components

Distributed information

The SBS technology is a distributed sensing technology. The localization of the measurements is possible through a "modified radar concept" using optical pulses launched in the sensing fibre. As long as the pulses propagate throughout the fibre, the Brillouin shift within the fibre is recorded as a function of time. The speed of light within an optical fibre being known, the time delay between the pulse launch and the detection of the Brillouin shift provides a direct information about the location of the interaction: the further the interaction takes place in the sensing fibre, the longer will be the time delay between the pulse launch and the detection of the interaction. One single fibre could therefore replace thousand of point sensors thanks to the distributed sensing concept. Brillouin-based fibre-optics distributed sensing technique can be split up in four processes:

- 1. Launch of optical pulses, so-called pump pulses.
- 2. Recording of back scattered Brillouin frequency as function of time. Step 1 and 2 are repeated until all Brillouin frequencies have been recorded. The result can be represented in a 3-D plot, see figure.
- 3. Processing of the Brillouin peak in the wavelength domain as function of time (distance).
- 4. Converting Brillouin peaks as function of time to temperature or strain as function of distance.

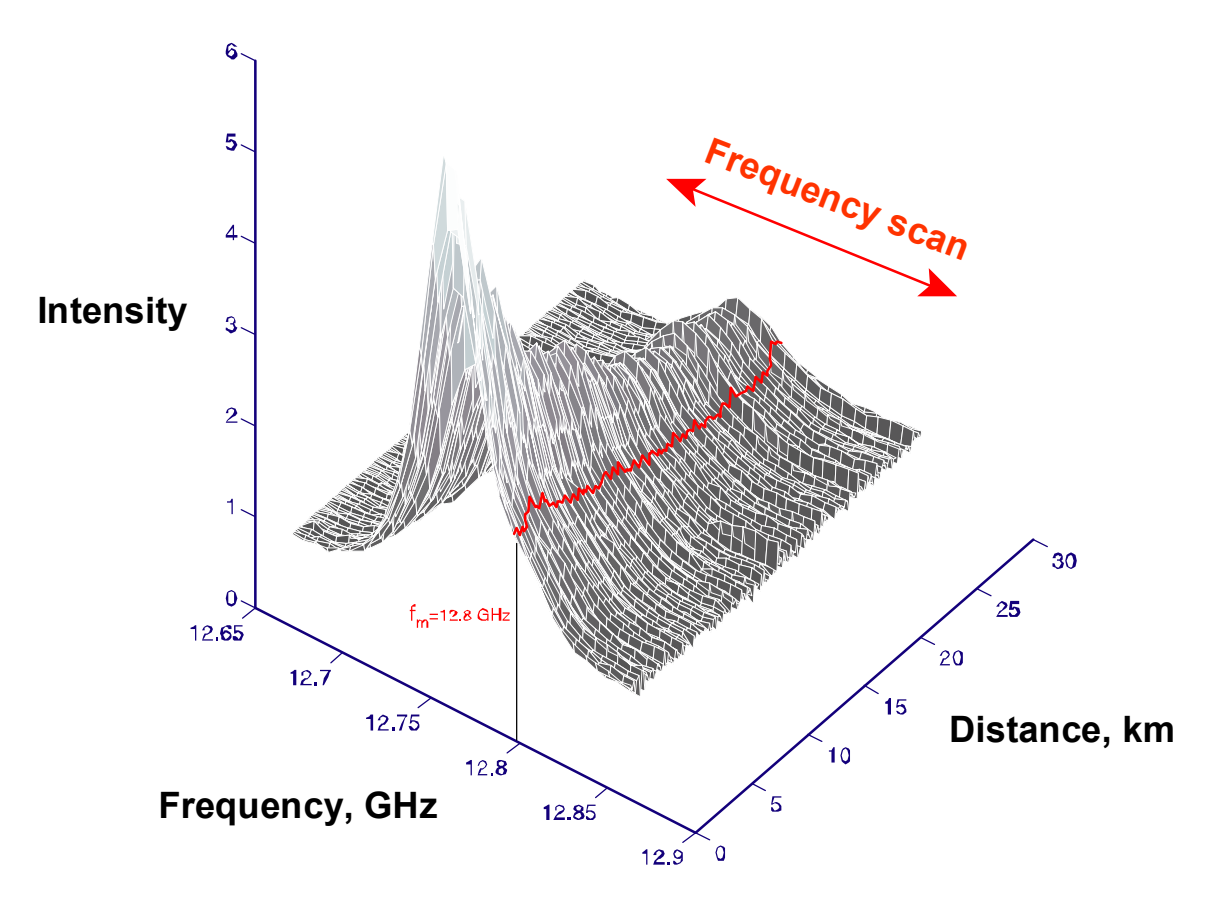


Figure 45: 3D representation of Brillouin shift measurements

Stimulated Brillouin scattering

Spontaneous Brillouin signal is very weak (100 x below the magnitude of the Rayleigh scattered light). As a consequence, a high-performance detection scheme is required. Conventional distributed Brillouin-based technologies are based on the measurement and the analysis of spontaneous Brillouin scattering and have therefore a limited range and resolution due to the low signal-to-noise ratio.

State-of-the-art technique relies on stimulated Brillouin scattering (SBS). This is achieved by using a Continuous Wave (CW) signal to increase the Brillouin gain in the fibre. The advantages are:

- Higer signal-to-noise ratio, higher accuracy
- Extended range and higher resolution
- Shorter acquisition time
- Higher flexibility (ex. threshold detection).

The CW Probe and pulses must be counter propagating throughout the sensing fibre, see Figure 46. This can be achieved by using a loop configuration – 2 optical fibres (Figure 47) or a single fibre configuration by using a mirror at the fibre end (Figure 48).

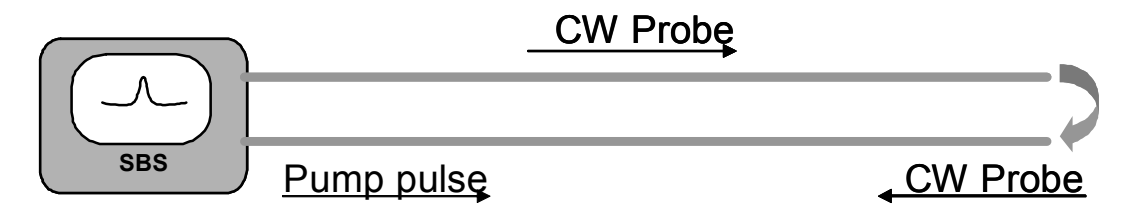


Figure 46: Principle-stimulated Brillouin scattering



Figure 47: Loop configuration



Figure 48: Single-fibre configuration

Temperature/strain cross-sensitivity

The temperature/strain cross-sensitivity is in practice not a problem and can be overcome, for example, by using an arrangement where the sensing fibre follows a double path in the structure to be monitored. One optical path being attached to the structure and thus subjected to both temperature and deformation, whereas the fibre being installed loose on the return path, measures only the temperature. Furthermore, when only the temperature profile is the relevant information, special fibre-optic cables can be used, which guarantee a strain-free installation.

Comparison: temperature monitoring using Brillouin sensing and FBG sensing

Table 8 shows the main differences between Brillouin sensing and FBG-sensing. Brillouin sensing allows similar as the Raman sensing a continuous monitoring along the length of the fibre, which can be a normal telecom fibre. The spatial resolution is in the range of 1 to 2 meters, and is much larger than the spatial resolution with FBG sensing (1 cm). The price of the interrogation unit is very high compared to the FBG interrogation unit.

| | Brillouin sensing | FBG sensing |
|----------------------------|-----------------------|----------------------|
| Measurement | Continuous | Discrete points |
| Spatial resolution | 1-5 m ⁽¹⁾ | 1 cm |
| Temperature resolution | 1-2 °C ⁽¹⁾ | 0.1 °C |
| Sensor | Normal telecom | Fibre Bragg Gratings |
| | fibre | |
| Price interrogation unit | 150 000 EUR | 9 000 EUR |
| Signal processing time per | 5-10 minutes | < 1 s |
| measurement cycle | | |

⁽¹⁾ Depending on the required sensing distance (1-25 km).

Table 8: Comparison between distributed temperature sensing using SBS and FBGs

Distributed temperature sensing using the Raman effect

The Fibre-optic Distributed Temperature Sensing (DTS) method using the Raman effect was developed at the beginning of the 1980s at Southampton University in England, UK. The DTS method is based on optical time-domain reflectometry (OTDR) and uses a technique derived from telecommunication cable testing.

In the DTS technique, a pulse laser is coupled to an optical fibre through a directional coupler. Due to the interaction between this laser pulse and the fibre, different light components will be backscattered. The backscattered light consists of different spectral components due to different interaction mechanism between the propagating light pulse and the optical fibre as has been shown in Figure 42. These backscattered lights include a Rayleigh component, a Brillouin component and a Raman component. Thermally influenced molecular vibrations cause the Raman backscattering component intensity. Thus its intensity depends on temperature. The Raman backscattered light has two components that lie symmetrically to the Rayleigh line: the Stokes line and Anti-Stokes line. The intensity of the Anti-Stokes line is lower than that of the Stokes line. The intensity of Stokes line weakly depends on temperature, whereas the intensity of the Anti-Stokes line is strongly related to temperature.

The fundamental technique employed by fibre-optic temperature measurement is filtering of the Stokes and the Anti-Stokes lines out of the backscattering light, based on the wavelength difference between these lines and the Rayleigh backscattering light. Using the ratio of the intensities of the Stokes and the Anti-Stokes lines eliminates external influences, such as age effects in the fibre and changes in light source or optical fibre.

Using principles similar to those employed in radar, the laser light is coupled to the optical fibre as a short light pulse in nanoseconds (ns). The intensities of both Raman lines are recorded with a time-resolving power of the order of 10 ns. The temperature is determined as an integral value for a short section of the optical fibre (about one meter) and the spatial co-ordinate is determined from the travel time of the propagating light pulse. Thus, it is possible to measure the temperature simultaneously along the entire length of the fibre. The spatial resolution is around 1 meter.

For better accuracy, a double-ended measurement is preferred. That is, a loop of fibre is used. The laser pulse is sent from one end of the fibre for the first measurement, after which, the laser source is switched to the other end of the loop for a second measurement. A geometric mean of the two measurements is calculated. The whole process takes about four minutes.

Comparison: temperature monitoring using Raman sensing and FBG sensing

The main differences are shown in Table 9. Raman sensing allows a continuous monitoring along the length of the fibre, which can be a normal telecom fibre. The spatial and temperature resolution are however not that good as with FBG sensing. This makes the Raman sensing less suitable to measure hot spots or to make accurate measurements. Also the price of the interrogation unit is much higher

for Raman sensing compared to FBG sensing. The Raman sensing can therefore only be seen as a competitive technology for very large sensing networks were a continuous monitoring along the length of the fibre is requested.

| | Raman sensing | FBG sensing |
|-----------------------------|--------------------------|----------------------|
| Measurement | Continuous | Discrete points |
| Spatial resolution | 1-8 m ⁽¹⁾ | 1 cm |
| Temperature resolution | 0.25-2 °C ⁽¹⁾ | 0.1 °C |
| Sensor | Normal telecom fibre | Fibre Bragg gratings |
| Price of interrogation unit | 55 000 EUR | 9 000 EUR |
| Signal processing time | 4 s to 10 minutes (2) | < 1 ms |
| per measurement cycle | | |

- (1) Depending on the required sensing distance (2-30 km).
- (2) Depending on required resolution and sensing distance.

Table 9: Comparison of distributed temperatures monitoring using Raman sensing and FBG sensing